Electronic Supplementary Material (ESI) for Dalton Transactions.

Turn off Luminescence Sensing, White – Light Emission and Magnetic Studies on Two-Dimensional lanthanide MOFs

Krishna Manna[a], Jean-Pascal Sutter[b]* and Srinivasan Natarajan[a]*

ELECTRONIC SUPPLEMENTARY INFORMATION

(a) Ms. Krishna Manna, Prof. Srinivasan Natarajan:
Framework solids Laboratory, Solid State and Structural Chemistry Unit
Indian Institute of Science
Bangalore 560012 (India)
Email: snatarajan@iisc.ac.in
Homepage: http://sscu.iisc.ac.in/people/frameworkslab/

(b) Prof. Jean-Pascal Sutter
Laboratoire de Chime de Coordination du CNRS
Université de Toulouse, CNRS
205 route de Narbonne, 31077 Toulouse (France)
E-mail : jean-pascal.sutter@lcc-toulouse.fr

Materials

The chemicals required for the synthesis of the compounds: $La(NO_3)_3.xH_2O$ (Ln= Y, Eu, Gd, Tb, Dy) propargyl bromide (80 wt% in toluene, 0.3% magnesium oxide as stabilizer) (Sigma-Aldrich); the compounds for the catalytic studies and 2, 5-dihyroxyterephthalic acid (TCI); THF, DMF, EtOH, KOH, MeOH, HCl (SDfine, India). The organophosphorus pesticides and nitroaromatics (Sigma) were used as purchased without any purifications. The water used was double distilled through a Millipore membrane. All the chemicals were used as purchased without any further purifications.

Synthetic procedure of the Ligand and MOF Compounds

The primary ligand, 2,5-bis(prop-2-yn-1-yloxy) terephthalic acid (2, 5 BPTA) was prepared by employing a known procedure.[1]

All the compounds were prepared by the sequential layering of three different solutions. The lanthanide nitrates, $Ln(NO_3)_3.xH_2O$, (0.05 mmol , ~0.020 g) was dissolved in 1 mL water (Solution **A**). Buffer solution (1 mL) was prepared by mixing 1:1 H_2O and DMF (Solution **B**). 2, 2′ Bipyridine (0.05 mmol, 0.008 g, compound **1a-5a**) or 1, 10 phenanthroline (0.05 mmol, 0.009 g, compound **1b-5b**) was dissolved in the buffer solution. The ligand 2,5-BPTA (0.05 mmol, 0.013 g) was dissolved in 1 mL of N, N-DMF (Solution **C**). In a Teflon-capped reaction vessel, solution **A** (1 mL) containing the lanthanide salt was added at the bottom. Then, 1 mL of solution **B** was carefully layered on the top of solution **A** followed by the addition of 1 mL of solution **C**. The reaction vessel was closed with a cap, and kept undisturbed in an oven at 75 ºC for 3-7 days. In the case of 2, 2′ bipyridine, large amount of cubic block shaped colourless crystals were isolated after 7 days. In case of 1, 10 phenanthroline, products with similar morphology came after 3 days. The yield in all cases was found to be in the range of ~60 - 70 % with respect to the lanthanide ions. Elemental analysis for all the compounds is listed in

Table S1. Powder X-ray diffraction (PXRD) studies (Figure S1) has confirmed the phase purity of the prepared samples. The mixed metal compounds were also prepared employing a similar procedure (Figure S2, S3).

Table S1A. Synthesis of compound 1-5 in layering method

Compound	Layer A	Layer B	Layer C	Temp (°C)	Time (days)	Shape and colour of crystal
Compounds 1a-5a	$Ln(NO_3)_3 \cdot xH_2O$ salt (0.020 g, 0.05 mmol) in 1 mL of water	2, 2′-bipyridine (0.008 g, 0.05 mmol) dissolved in the 1 mL buffer solution of DMF and water	2,5 BPTA (0.013 g, 0.05 mmol) in 1 mL of DMF	**75**	**7**	Colourless, cubic
Compounds 1b-5b	$Ln(NO_3)_3 \cdot xH_2O$ salt (0.020 g, 0.05 mmol) in 1 mL of water	1, 10 phenanthroline, (0.009 g, 0.05 mmol) in the 1 mL buffer solution of DMF and water	2,5 BPTA (0.013 g, 0.05 mmol) in 1 mL of DMF	**75**	**3**	Colourless, cubic

Table S1B Elemental Analysis of Compound **1-5 (a, b)**

Compound	%C		%H		%N		%O	
	As Synthesized	**Calc.**	**As Synthesized**	**Calc.**	**As Synthesized**	**Calc.**	**As Synthesized**	**Calc.**
Compound **1a**	55.34	55.46	3.12	3.3	4.35	4.17	23.07	23.83
Compound **2a**	49.87	50.69	2.93	3.02	4.01	3.81	21.95	21.78
Compound **3a**	50.19	50.33	2.86	3.00	3.85	3.79	21.41	21.63
Compound **4a**	50.13	50.22	2.53	2.99	4.01	3.78	21.55	21.58
Compound **5a**	49.34	49.98	2.71	2.98	3.9	3.76	21.6	21.47
Compound **1b**	56.84	56.99	2.99	3.19	4.1	4.03	23.41	23.01
Compound **2b**	52.71	52.26	2.59	2.92	3.81	3.69	20.71	21.09
Compound **3b**	52.06	51.89	2.53	2.9	3.86	3.67	20.69	20.95
Compound **4b**	52.09	51.78	2.78	2.9	3.76	3.66	20.21	20.91
Compound **5b**	51.76	51.54	2.5	2.88	3.66	3.64	20.85	20.80

Table S2a Selected bond lengths (Å) and bond angles (deg) for **3a,** Gd containing 2, 2′-bipyridine MOF.

Table S2b Selected bond lengths (Å) and bond angles (deg) for **5b,** Dy containing 1,10-phenanthroline MOF

Compound **3a**			
Bond length(Å)		**Bond angle (°)**	
Gd1-O1_4	2.36(4)	O1_4-Gd1-O1_5	76.71(15)
Gd1-O1_5	2.36(4)	O1_4-Gd1-N1_2	147.89(17)
Gd1-N1_2	2.54(5)	O1_4-Gd1-N1'_2	147.89(17)
Gd1-O1_3	2.34(5)	O1_3-Gd1-O1_4	72.44(15)
Gd1-N1'_2	2.57(4)	O1_3a-Gd1-O1_4	90.66(13)
Gd1-O1_4	2.36(4)	O2_3_a-Gd1-O1_4	82.06(16)
Gd1-N1_2a	2.49(3)	O1_3-Gd1-N10_2	90.66(13)
Gd1-N1'_2a	2.50(6)	O1_4-Gd1-N10_2	131.92(16)
Gd1-O2_3_a	2.40(4)	O1_4-Gd1-O2_5_b	73.88(13)
Gd1-O1_4_b	2.34(5)	O1_3-Gd1-O2_5_b	139.57(13)
Gd1-O2_5_b	2.58(2)	O1_4-Gd1-O2_4_b	122.86(14)
Gd1-O2_4_b	2.38(4)	O1_3-Gd1-O1_4_b	77.95(14)
Gd1-O1_4_b	2.49(5)	O1_4-Gd1-O2_5_b	73.44(14)
Gd1-O2_5_b	2.45(5)	O1_3-Gd1-O2_4_b	68.36(15)
Dy1-O1_5_c	2.38(4)	O1_3-Gd1-N1_2	80.24(16)
Dy1-O2_5_c	2.43(3)	O1_3-Gd1-N1'_2	85.40(13)
		O1_3a-Gd1-N1_2	134.47(16)
		O1_3-Gd1-O2_5_c	77.20(15)
		O1_3a-Gd1-N1'_2	76.32(15)
		O1_4-Gd1-N1_2	147.39(16)
		O2_3_a-Gd1-O1_5	128.43(14)
		O1_4-Gd1-N10_2	147.33(16)
		O1_4_b-Gd1-O1_5	68.85(14)
		O2_3_b-Dy1-O1_4	72.47(14)
		O2_4_b-Gd1-O1_5	79.37(13)
		O1_4-Dy1-O1_4_b	74.47(12)
		O1_4-Dy1-O2_4_b	136.34(14)
		O1_4-Dy1-O2_5_b	119.74(14)
		N1_2-Dy1-N1'_2c	63.00(18)
		O1_3_a-Gd1-N1_2	99.89(13)
		O1_4-Dy1-O2_5_c	73.39(15)
		O2_3_a-Gd1-N1_2	83.45(16)
		N1_2-Dy1-N10_2	65.24(17)
		O1_4_b-Gd1-N1_2	131.89(16)
		O2_3_b-Dy1-N1_2	137.42(16)
		O2_4_b-Gd1-N1_2	77.24(18)
		O1_4_b-Dy1-N1_2	120.29(18)
		O2_5_b-Gd1-N1_2	139.85(15)
		O2_4_b-Dy1-N1_2	68.80(15)
		O1_3_a-Gd1-N1'_2	81.52(15)
		O1_3_c-Dy1-N1_2	144.87(15)
		O2_3_a-Gd1-N1'_2	75.33(15)
		O2_3_c-Dy1-N1_2	75.03(14)
		O1_4_b-Gd1-N1'_2	107.70(15)
		O2_3_b-Dy1-N10_2	76.12(16)
		O2_4_b-Gd1-N1'_2	67.56(18)
		O1_4_b-Dy1-N10_2	88.50(13)
		O2_5_b-Gd1-N1'_2	77.00(15)
		O2_4_b-Dy1-N10_2	66.90(17)
		O1_3_a-Gd1-O2_3_a	53.13(14)
		O1_5_c-Dy1-N10_2	79.99(14)
		O2_3_a-Gd1-O1_4_b	136.56(13)
		O2_5_c-Dy1-N10_2	122.78(13)
		O1_3_a-Gd1-O2_4_b	143.77(19)
		O2_3_b-Dy1-O1_4_b	73.87(14)
		O1_3_a-Gd1-O2_5_b	124.03(15)
		O2_3_b-Dy1-O2_4_b	142.28(14)
		O2_3_a-Gd1-O1_4_b	153.50(14)
		O2_3_b-Dy1-O1_5_c	74.58(14)
		O2_3_a-Gd1-O2_4_b	143.74(16)
		O2_3_b-Dy1-O2_5_c	115.08(14)
		O1_4_b-Gd1-O2_5_b	82.41(15)
		O1_4_b-Dy1-O2_4_b	51.51(14)
		O1_4_b-Gd1-O2_4_b	50.12(15)
		O1_4_b-Dy1-O1_5_c	148.18(15)
		O1_4_b-Gd1-O2_5_b	72.98(15)
		O1_4_b-Dy1-O2_5_c	148.38(13)
		O2_4_b-Gd1-O2_5_b	92.28(2)
		O2_4_b-Dy1-O2_5_c	142.28(14)
a = 1-x, 1-y, 1-z		O1_5_c-Dy1-O2_5_c	132.58(16)
b ≡ 1-x, 1-y, 1-z b = 1-x, 2-y, 1-z c = 1-x, 2-y, 1-z			

Table S4 Hydrogen bonding for **3a** compound

D-H···A (Å)	d(D-H) (Å)	d(H-A) (Å)	d(D···A) (Å)	∠DHA (°)	Symmetry transforms
Compound **3a**					
C3'_2–H3'_2···O1_6	0.95	2.57	3.49(9)	165.00	x,y,1+z
C2_6–H2A_6···O1_8	0.99	2.44	3.42(6)	170.00	1-x,1-y,1-z
C2_6–H2A_6···O1_7	0.99	2.56	3.52(6)	165.00	1-x,1-y,1-z
C4_6–H4_6···O1_1	0.95	2.10	3.04(19)	170.00	1+x,y,z
C4_9–H4_9···O1_1	0.95	2.19	3.09(2)	157.00	1-x,2-y,-z

Compound	ν(≡C–H) (cm^{-1})	ν(C≡C) (cm^{-1})	ν(COO) acid (cm^{-1})	ν(C=C) (cm^{-1})	ν(C=N) (cm^{-1})	$\nu(O–H)_{str}$ non coordinated H_2O (cm^{-1})	ν(C-H) Aromatic
2,5 BPTA	~3261	~2126	~1693		-	-	
Compound **1a-5a**	~3243	~2117	~1657	~1584	~1528	~3640	~3060
Compound **1b-5b**	~3309	~2127	~1670	~1610	~1539	~3400-3300-	~3065
2, 2′ Bipyridine	-	-	-	~1578	~1557	-	~3052
1, 10 phenanthroline	-	-	-	~1644	~1586	~3363	~3056

Table S5. List of important IR bands observed in **1-5(a, b)**

The IR spectra of the ligand, 2, 5 BPTA, (Figure S5a) exhibits a sharp band at 3261 cm^{-1}, which can be assigned to the stretching of the alkyne ≡C–H group. The band at 2126 cm^{-1} corresponds to the C≡C stretching. A broad band in the 3000-2780 cm^{-1} corresponds to the aromatic C–H stretching from the benzene ring and the stretching of the methylene group. The IR spectra of 2, 2′ - bipyridine and 1, 10 – phenanthroline shows aromatic stretching bands at 3052 and 3056 cm^{-1}. The typical C=C and C=N frequency appears at 1584 and 1528 cm^{-1} for bipyridine and 1610, 1539 cm^{-1} for phenanthroline. For the compound **1a-5a**, a sharp peak at ~3640 cm^{-1} corresponds to the stretching frequency of the lattice water molecule. Also, the C=N stretching frequency appears to be red shifted to 1528 cm^{-1} for the electron donation from N to the metal centres. For compounds **1b-5b,** also, the C=N bond appears at ~1539 cm^{-1} which is red shifted from the uncoordinated phenanthroline. There are previous reports in this kind of observations.[2–4] In addition to these, other IR bands that corresponds to -C=O, ≡C–H, C≡C etc. have been observed. All the observed IR bands were listed in Table S5.

Table S6. List of UV-Vis spectra observed in **1-5 (a, b)**

Sl No:	Compound	Wavelength (nm)	Optical transition
UV-Vis			
1	Ligand	278 340	π-π* n-π*
2	2, 2′ bipyridine	232 285	π-π* n-π*
3	1, 10 phenanthroline	256 330	π-π* n-π*
4	Compound **1a-5a**	~280 312-365	π-π* n-π*
5	Compound **1b-5b**	~290 311-364	π-π* n-π*

The room temperature UV-Vis spectra of the ligand (Figure S6a) showed absorption bands corresponding to the л–л* (278 nm) and the n–л* (340 nm) transitions. For the 2, 2′ bipyridine, the bands are observed at λ_{max} 235 and 282 nm for the л–л* and n–л* transitions. Compared to 2,2′-bipyridine, 1,10-phenanthroline possesses a more rigid geometry with the three aromatic rings substantially coplanar and the two nitrogen atoms in juxtaposition.[5] This means that with a greater extent of conjugation, less energy is needed (and the longer the wavelength of radiation) to excite an electron for the л → л* transition, so that extensively conjugated compounds can absorb longer wavelength. Here, the rigidity of phenanthroline is reflected in the structured UV absorption spectral features, where we observed the λ_{max} 256 and 330 nm for the л–л* and n–л* transitions.[6,7] Compound **1a-5a** exhibited a red-shift in the UV-Vis spectra of both the л–л* and n–л* transitions at 280 and 320-350 nm. On the other hand, the UV-Vis spectra of the phenanthroline complexes showed the bands at ~290 nm for the л → л* transition and 311-364 nm for the n–л* transitions.[8] Here in individual peaks are not observed for the ligand, metal and the bipyridine; a overall broad band is observed due to the overlapping of the absorption spectra. Similar kind of observations has been made before.[9] All the observed UV-Vis band is tabulated in Table S6.

Table S7. CIE chromaticity coordinates (x, y) for $Y_{0.98-x}Tb_{0.02}Eu_x$– MOF material samples with different Eu^{3+} concentrations ($0 < x < 4.0$) and $Y_{0.94-x}Tb_{0.06}Eu_x$– MOF material samples

$Y_{1-0.02-x}Tb_{0.02}Eu_x$ (x = 0.0, 0.5, 1.0, 2.0, 3.0, 4.0 %)			
Sample code	**CIE X**	**CIE Y**	**CCT (K)**
0.0% Eu	0.252	0.455	7885
0.5 % Eu	0.286	0.423	6986
1.0 % Eu	0.303	0.391	6560
2.0 % Eu	**0.33**	**0.345**	**5604**
3.0 % Eu	0.370	0.312	3766
4.0 % Eu	0.411	0.295	2273
$Y_{1-0.06-x}Tb_{0.06}Eu_x$ (x = 0.0, 0.05, 0.10, 0.20, 0.30, 0.40 %)			
0.0% Eu	0.22	0.431	9444
0.05 % Eu	0.291	0.391	7035
0.1 % Eu	**0.332**	**0.331**	**5517**
0.2 % Eu	0.401	0.312	2271
0.3 % Eu	0.435	0.295	1883
0.4 % Eu	0.491	0.274	2291

Table S8. Comparison of the literature reported white light emitting MOF materials with the present White light emitting materials

MOFs	Excitation wavelength (nm)	CIE chromaticity (x, y)	CCT (K)	Quantum yield (%)	Reference
$[Dy(TETP)(NO_3)_3]\cdot 4H_2O$	365	0.33, 0.35	-	58%	[10]
$[Zn_3(TCPB)_2(H_2O)_2]\cdot 2H_2O\cdot 4DMF$ 1.05% Eu and 1.56% Tb	254	0.3292, 0.3543	-	-	[11]
NKU-114@9-AA	365	0.34, 0.32	5101	42.07%	[12]
$Eu_{0.005}Tb_{0.095}$-$Bi_{0.9}$-MOF	325	0.33, 0.31	-	-	[13]
$Eu_{0.09}Tb_{0.21}$@1	365	-	-	48.5%	[14]
$[Ir(ppy)_2(bpy)]^+$@$[(CH_3)_2NH_2]_{15}[(Cd_2Cl)_3(TATPT)_4]\cdot 12DMF\cdot 18H_2O$	370	0.31, 0.33	5409	84.5 %	[15]
BGR MOF	360	0.333, 0.336	-	-	[16]
$Tb_{0.31179}Eu_{0.1099}Gd_{0.5782}$-SURMOF	360	0.331, 0.329	5614	-	[17]
ZJU-1:1.0%Tb^{3+},2.0%Eu^{3+}	312	0.32, 0.31		6.11	[18]
$[Eu(H_2O)_2(OH)(Hsfpip)]\cdot H_2O$	380	0.31, 0.35		16.5	[19]
$Y_{0.96}Tb_{0.02}Eu_{0.02}$ (BPTA-bpy)	345	0.334 0.346	5432	28	[20]
$Y_{0.96}Tb_{0.02}Eu_{0.02}$ (BPTA-bpy)	350	0.33, 0.345	5604	31	this work
$Y_{0.939}Tb_{0.06}Eu_{0.001}$(BPTA-phen)	350	0.332, 0.331	5517	43	this work

LOD calculation

The luminescence intensity of the compound was plotted as a function of cation concentration. The limit of detection (LOD) is given by: LOD = 3σ/m, where σ is the standard deviation of the blank measurements without adding the anion and m is the slope of the linear plot.

Table S9. Standard deviation and detection limit calculation for the azinphos-methyl pesticide and nitroaromatics sensing using the Tb and Eu MOFs.

Blank readings of MOFs (without analyte)	Luminescence intensity	Standard deviation (σ)	Slope from the graph (m)	Detection limit (3σ/m)	Limit of detection (LOD) (ppb)
PESTICIDE SENSING					
Tb phen-MOF					
Reading 1	865249	11.2	1.008×10^{7} mM^{-1}	3.33×10^{-6} mM	1.06
Reading 2	865263				
Reading 3	865251				
Reading 4	865239				
Reading 5	865271				
Eu-phen-MOF					
Reading 1	260676	20.84	4.07×10^{6} mM^{-1}	1.53×10^{-5} mM	4.93
Reading 2	260678				
Reading 3	260698				
Reading 4	260743				
Reading 5	260640				
NITROAROMATICS SENSING					
Tb bpy-MOF					
Reading 1	522106	24.61	1.75×10^{7} mM^{-1}	4.21×10^{-6} mM	0.97
Reading 2	522171				
Reading 3	522116				
Reading 4	522128				
Reading 5	522157				
Eu bpy-MOF					
Reading 1	526117	27.89	1.53×10^{7}	5.46×10^{-6}	1.23
Reading 2	526112				
Reading 3	526137				
Reading 4	526157				
Reading 5	526188				

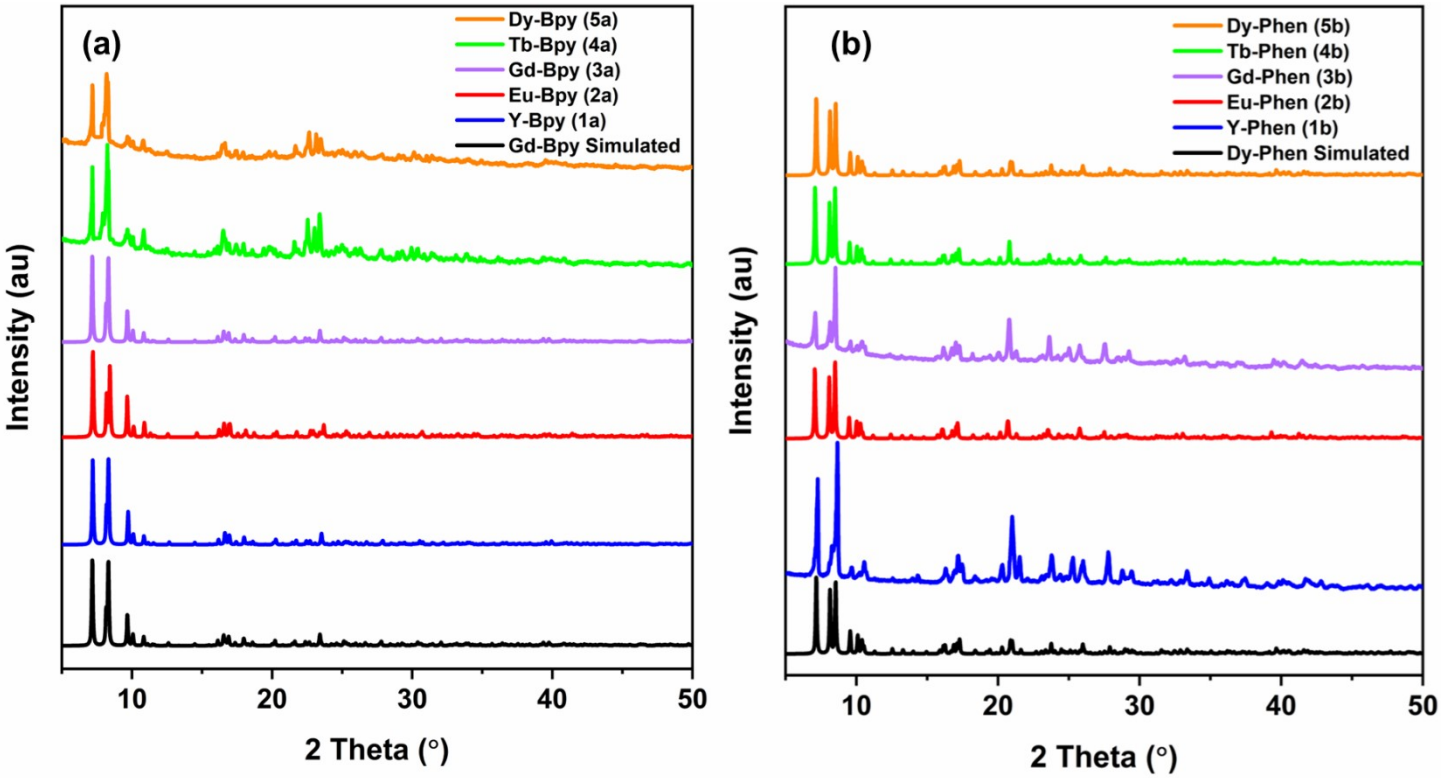

Figure S1. Experimental and simulated PXRD patterns of (a) 3a compound and (b) 5b compound. Note the experimental PXRD pattern of other compounds exactly matches with the simulated pattern of **3a** and **5b**.

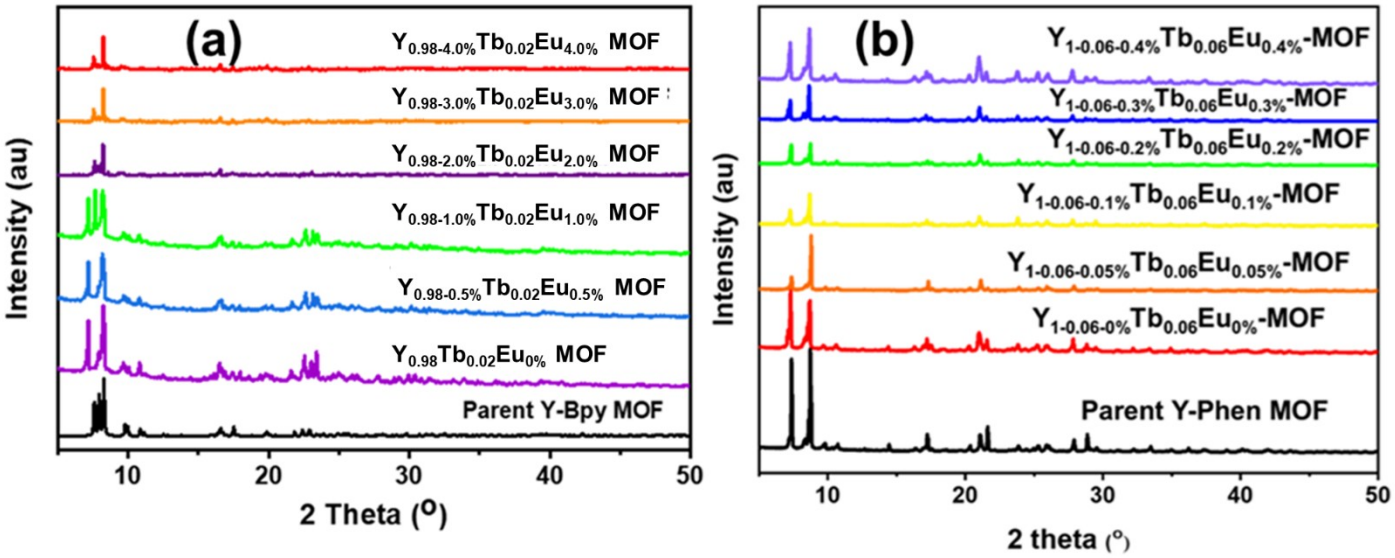

Figure S2. PXRD patterns of **(a)** $Y_{0.98-x\%}Tb_{0.02}Eu_{x\%}$– MOF samples (bpy series) and **(b)** $Y_{0.94-x\%}Tb_{0.06}Eu_{x\%}$– MOF samples (phen series), confirming the structural integrity

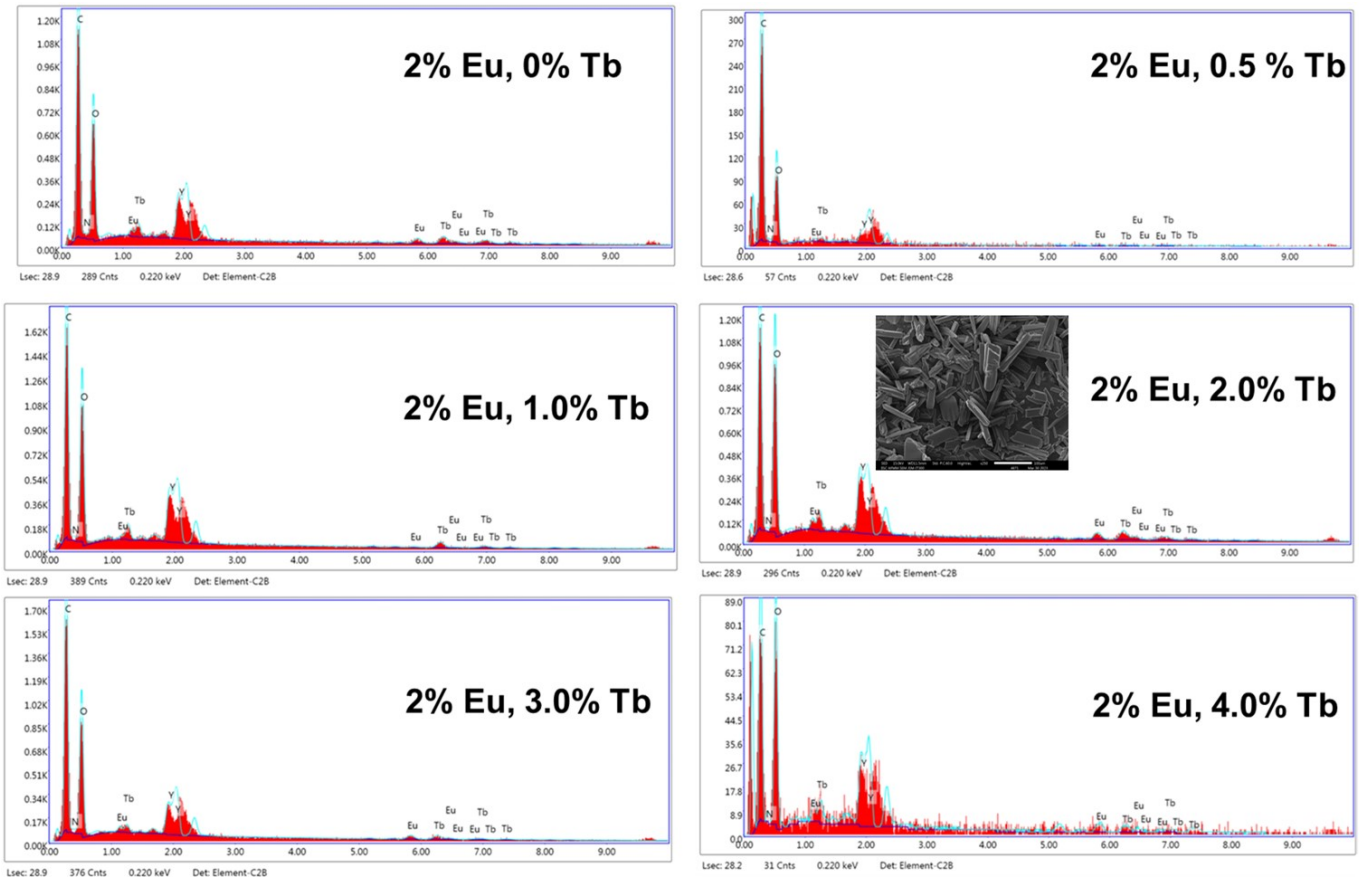

Figure S3. EDX mapping of all dopped Y – bipyridine MOFs ($Y_{1-0.02-x}Tb_{0.02}Eu_x$ (x = 0.0, 0.5, 1.0, 2.0, 3.0, 4.0 %)) samples , SEM image of 2%Tb, 2% Eu, Y- bipyridine MOF

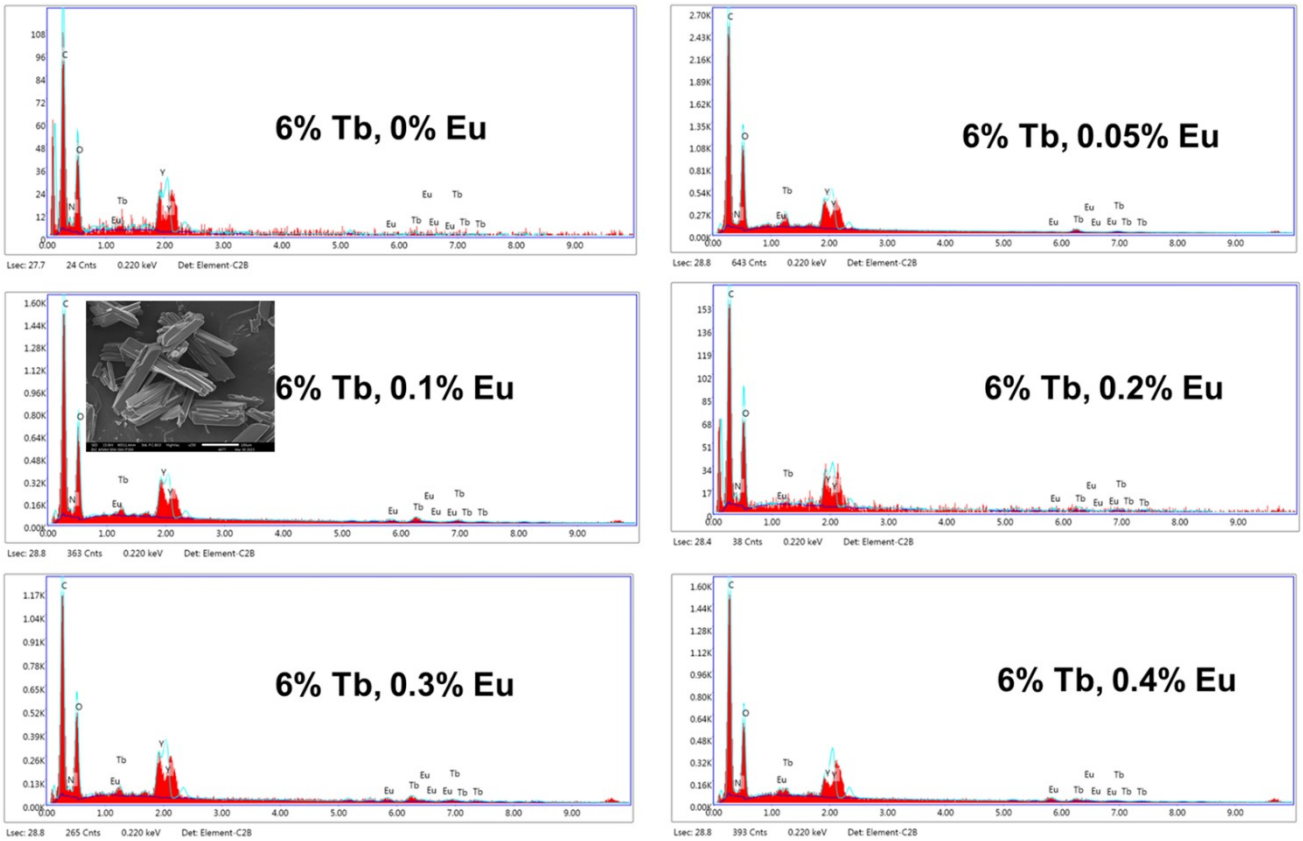

Figure S4. EDX mapping of all dopped Y – bipyridine MOFs ($Y_{1-0.06-x}Tb_{0.06}Eu_x$ (x = 0.0, 0.05, 0.1, 0.2, 0.3, 0.4 %)) samples, SEM image of 6%Tb, 0.1% Eu, Y- 1, 10 phenanthroline MOF

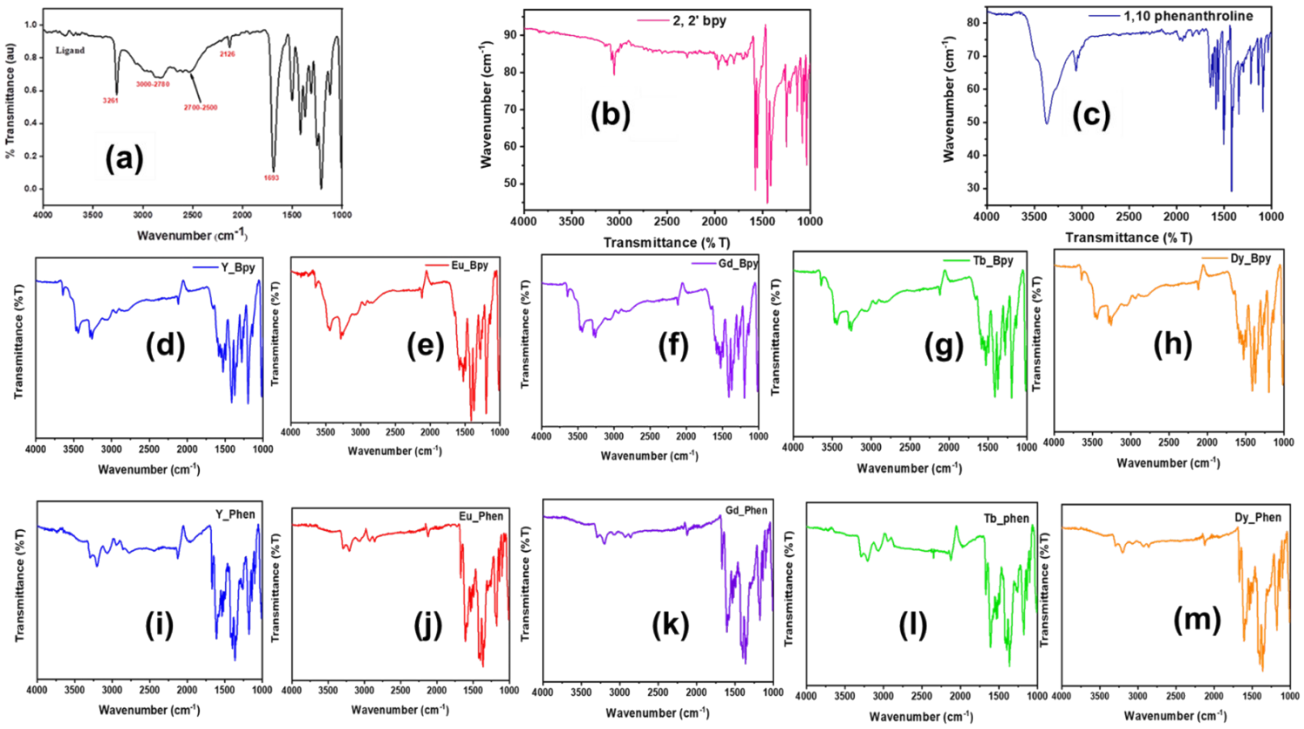

Figure S5. Infrared spectra of ligand (2, 5 BPTA) **(a)**, 2, 2′ - bipyridine **(b)**, 1, 10 – phenanthroline **(c)** Compounds **1a-5a (d-h)** and Compounds **1b-5b (i-m).**

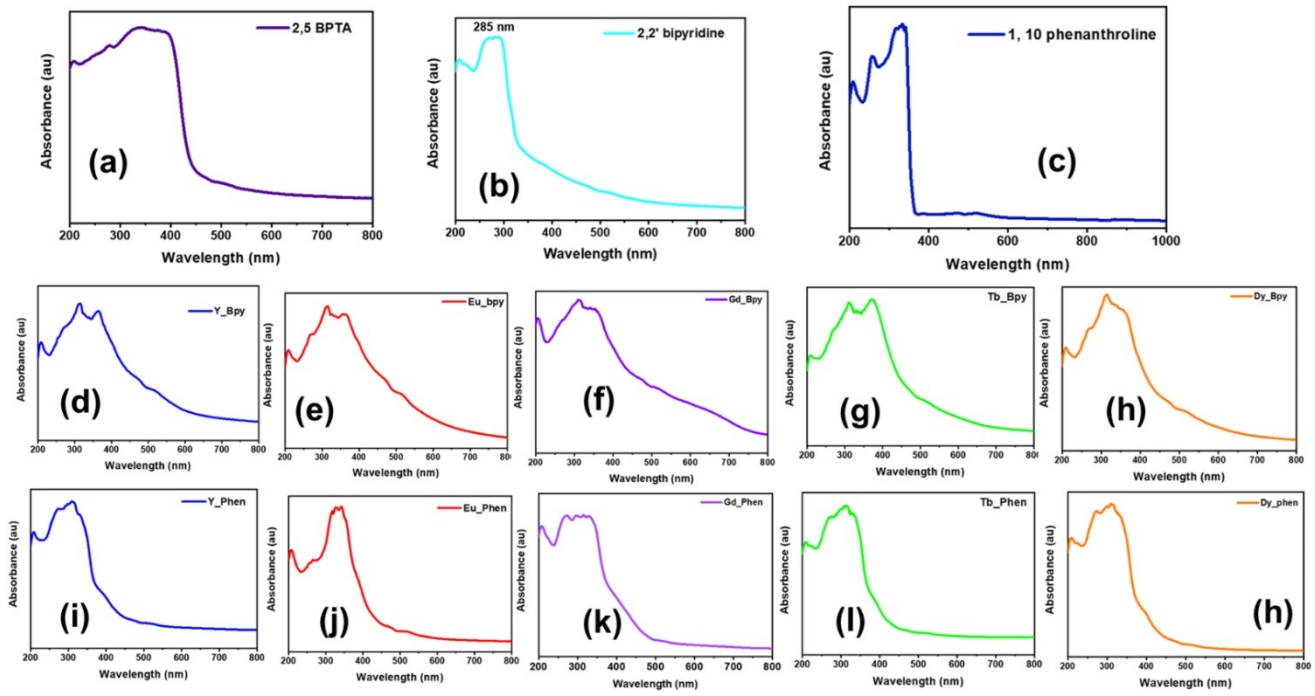

Figure S6. The solid-state UV−Vis absorption spectrum of compound **1-5 (a,b)**.

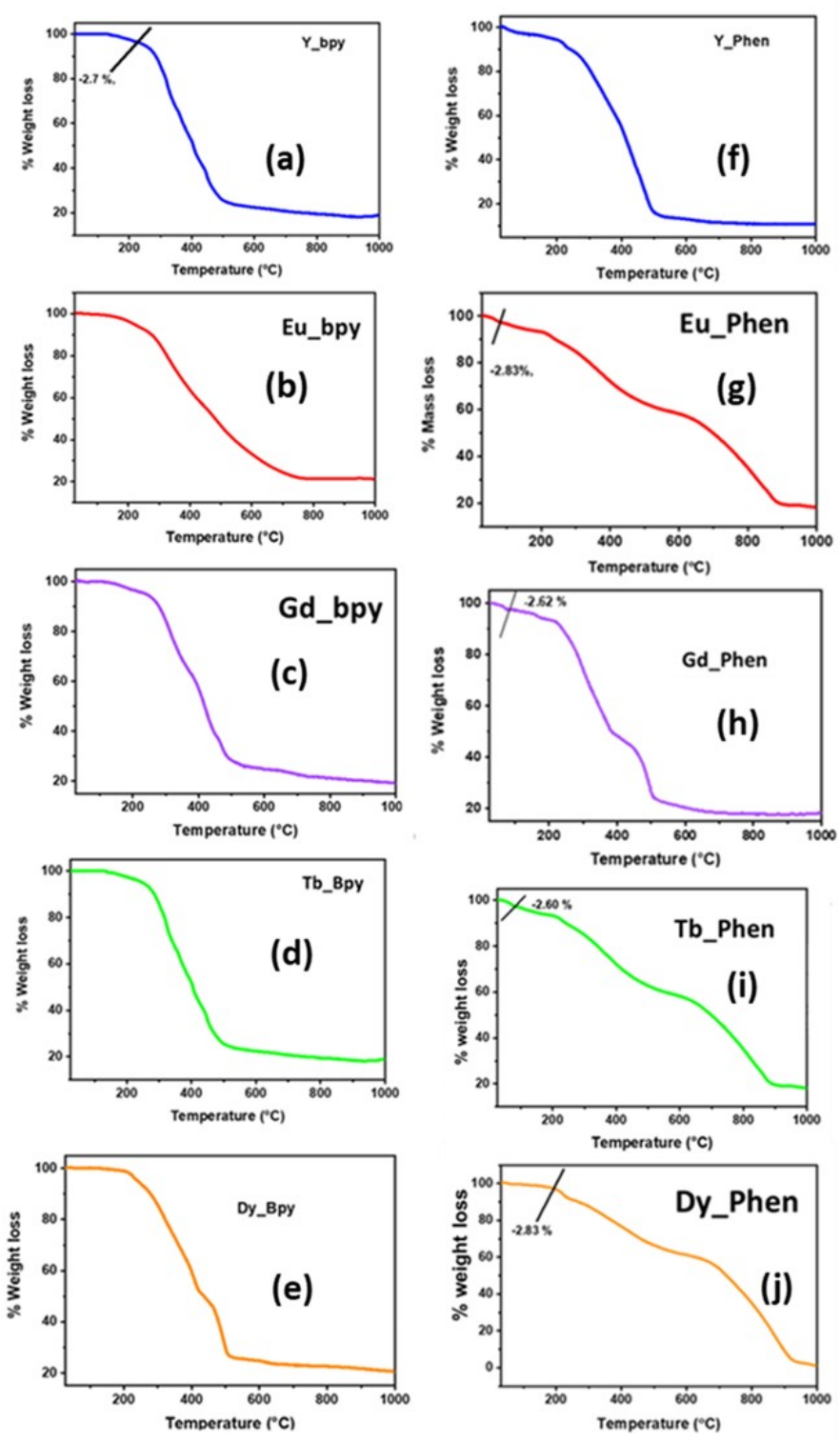

Figure S7. Thermogravimetric analysis curve (TGA) curve of compounds **1a-5a (a-e)** and compounds **1b-5b (f-j).**

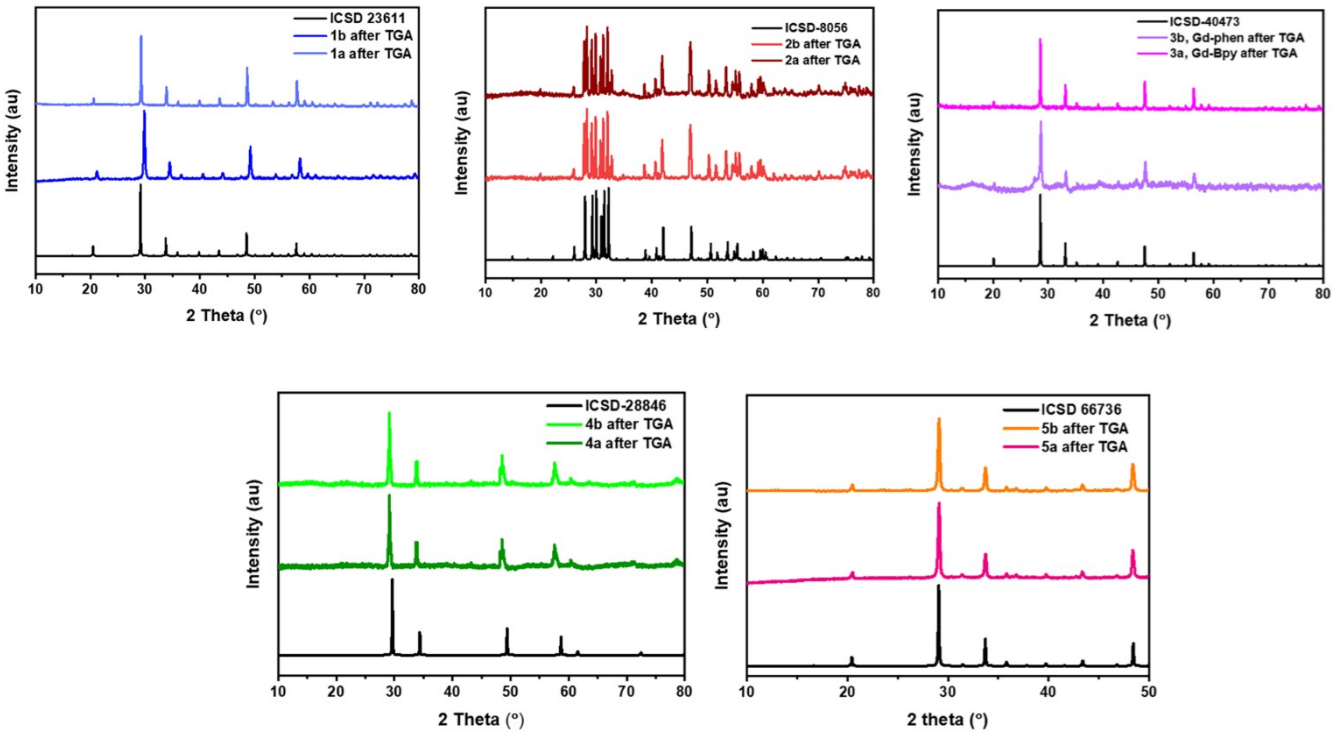

Figure S8. PXRD analysis after thermogravimetric analysis curve (TGA) curve of Compounds **1-5 (a, b).**

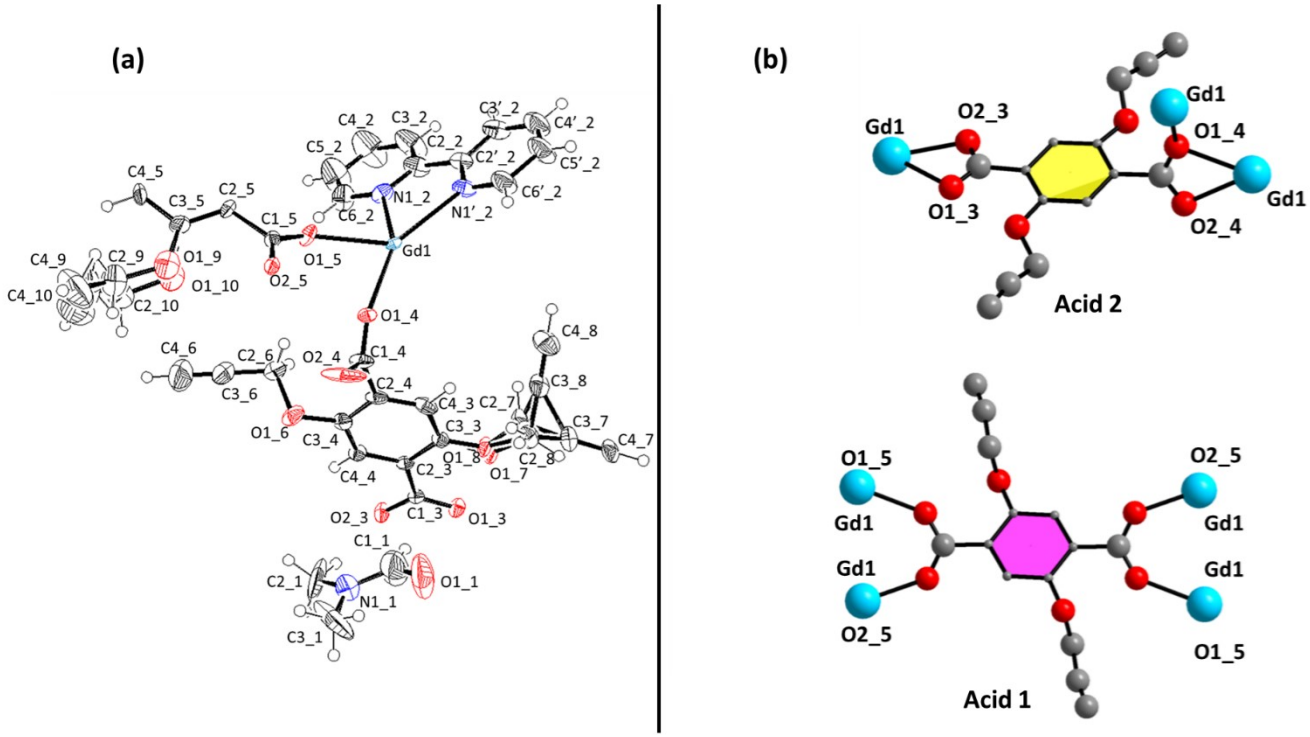

Figure S9. (a) Asymmetric unit of **3a (**Gd-bipyridine compound**)** (Thermal ellipsoid with 50% probability); (b) The various coordination modes of the 2, 5 BPTA anions in Gd MOF, acid 1 and acid 2

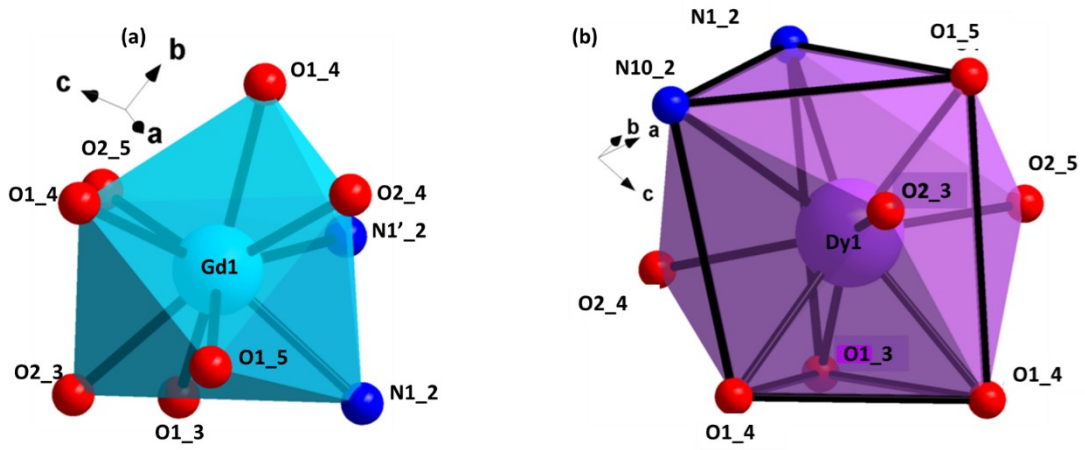

Figure S10. Metal coordination of **(a) Gd** bpy **(3a**) MOF, $[Gd(BPTA)_{1.5}(Bpy)]\cdot 0.5DMF$ capped square antiprismatic geometry and **(b) Dy** phenanthroline **(5b)** MOF, $[Dy(BPTA)_{1.5}(Phen)]\cdot 0.5DMF$ tricapped trigonal prismatic geometry.

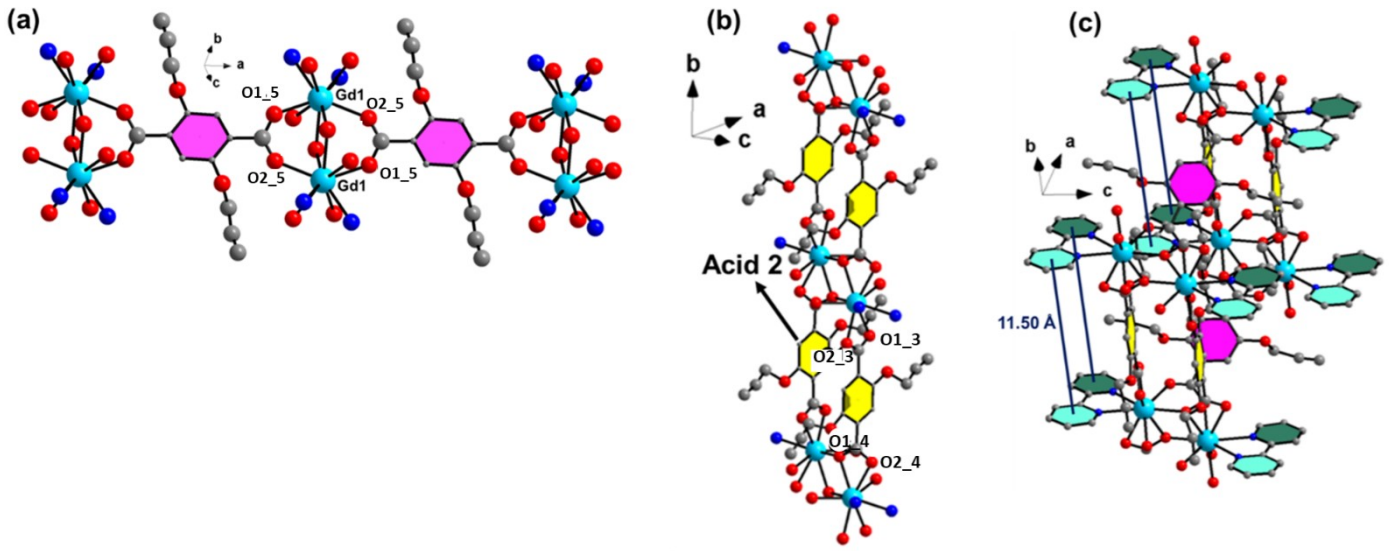

Figure S11. (a) 1D chain formation by acid – 1 **(b)** 1D chain formation by acid 2 **(c)** distance between the bipyridine units in a single layer **(d)** The lattice water molecule interactions with layers.

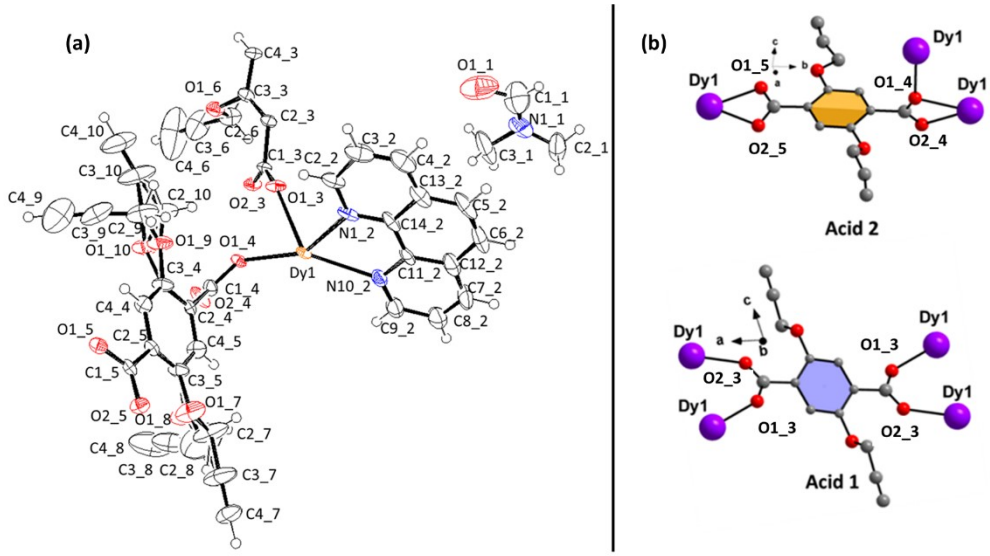

Figure S12. (a) Asymmetric unit of **5b** (Dy-phen compound) (Thermal ellipsoid with 50% probability); **(b)** The various coordination modes of the 2, 5 BPTA anions in Dy MOF, acid 1 and acid 2

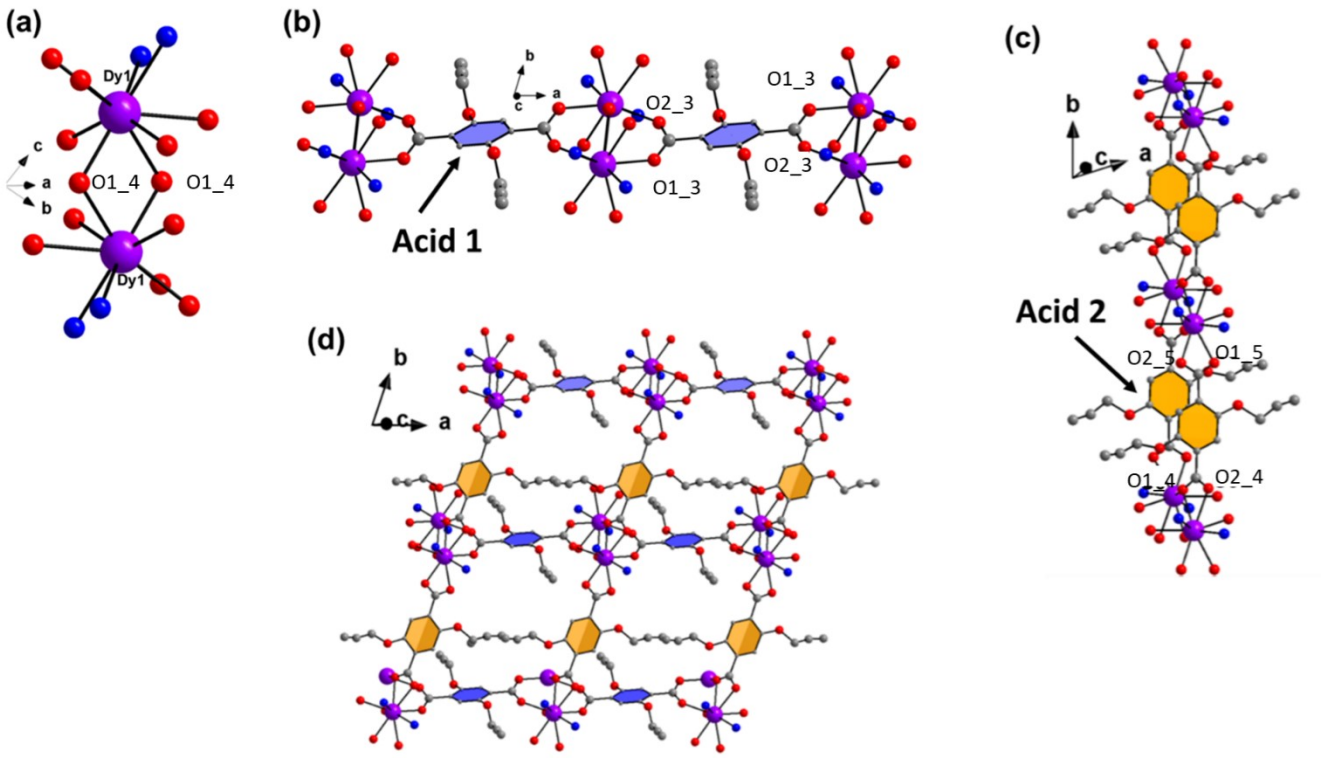

Figure S13. (a) Dimeric unit formed by O6 atom **(b)** 1D chain propagation by the Acid 1-unit **(c)** 1D chain propagation by Acid 2 (d) 2D layer formation in **5b**; phenanthroline containing MOF

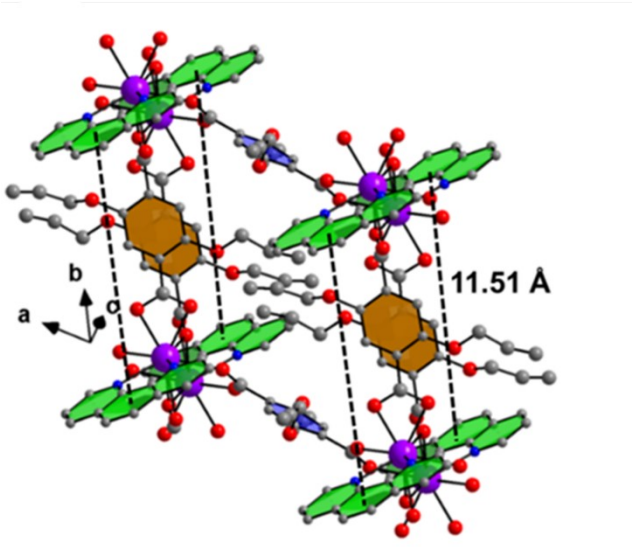

Figure S14. Distance between 1, 10 phenanthrolines in a single layer

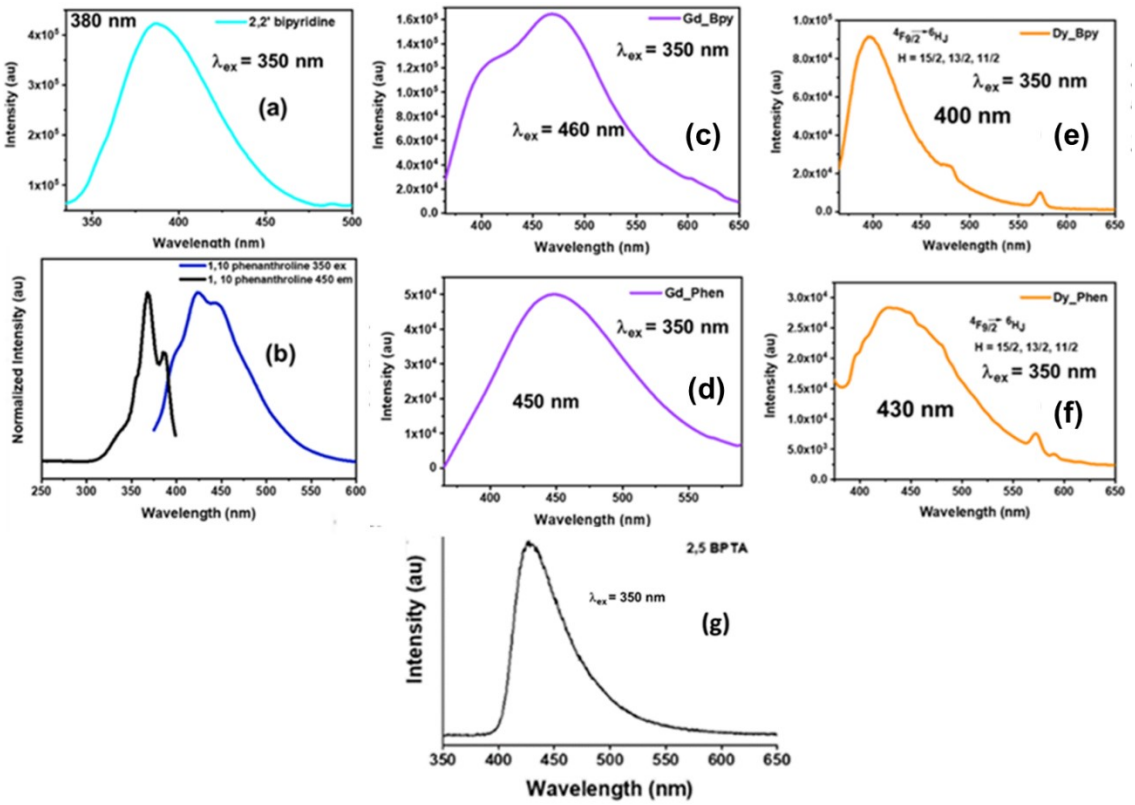

Figure S15. Room-temperature photoluminescence spectra for 2, 2′ bipyridine, 1, 10 phenanthroline, compound **3a** (c), **3b** (d), **5a** (e), **5b** (f) and the ligand (g)

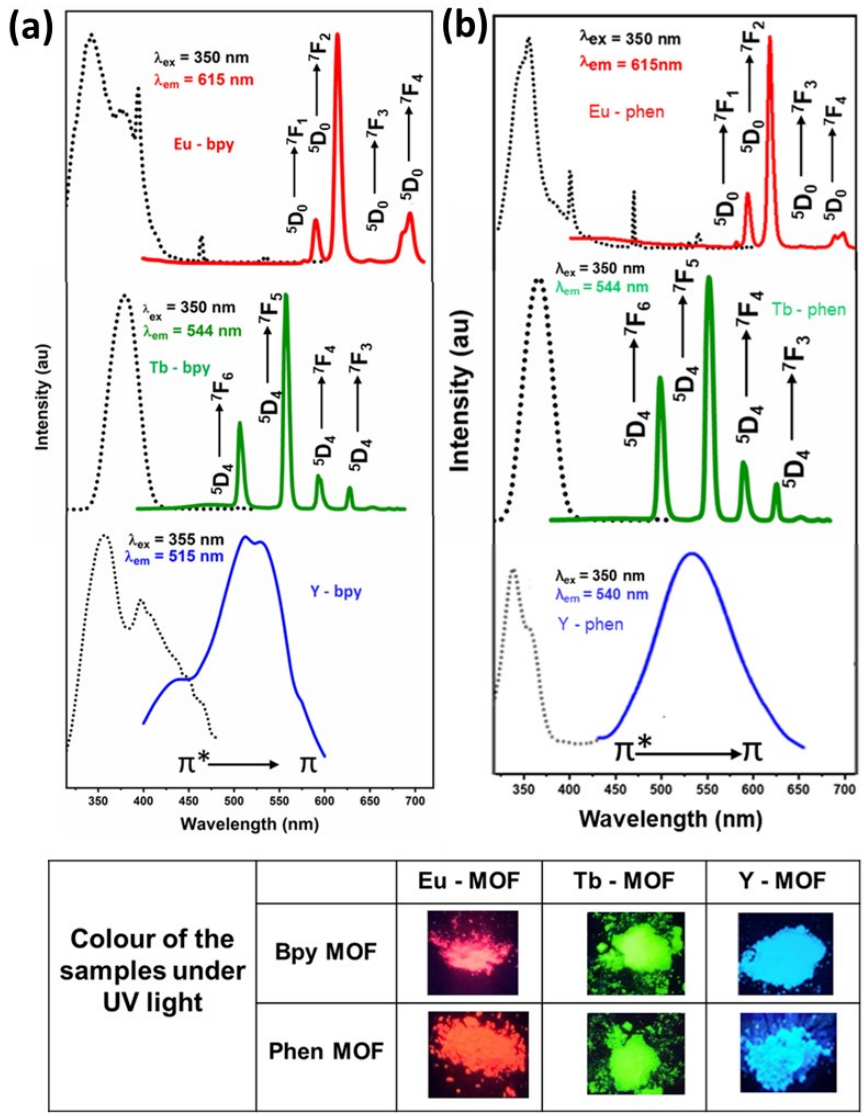

Figure S16. Excitation (black dotted) and emission spectra of Eu-MOF, Tb-MOF, Y-MOF in the solid-state Inset: Photograph showing the luminescence colour of the MOFs under long UV lamp. Note the characteristic red, green and blue colour for Eu^{3+}, Tb^{3+} and the Y containing compound, **(a)** 2, 2′ Bipyridine containing compounds **(b)** 1, 10 phenanthroline containing compounds.

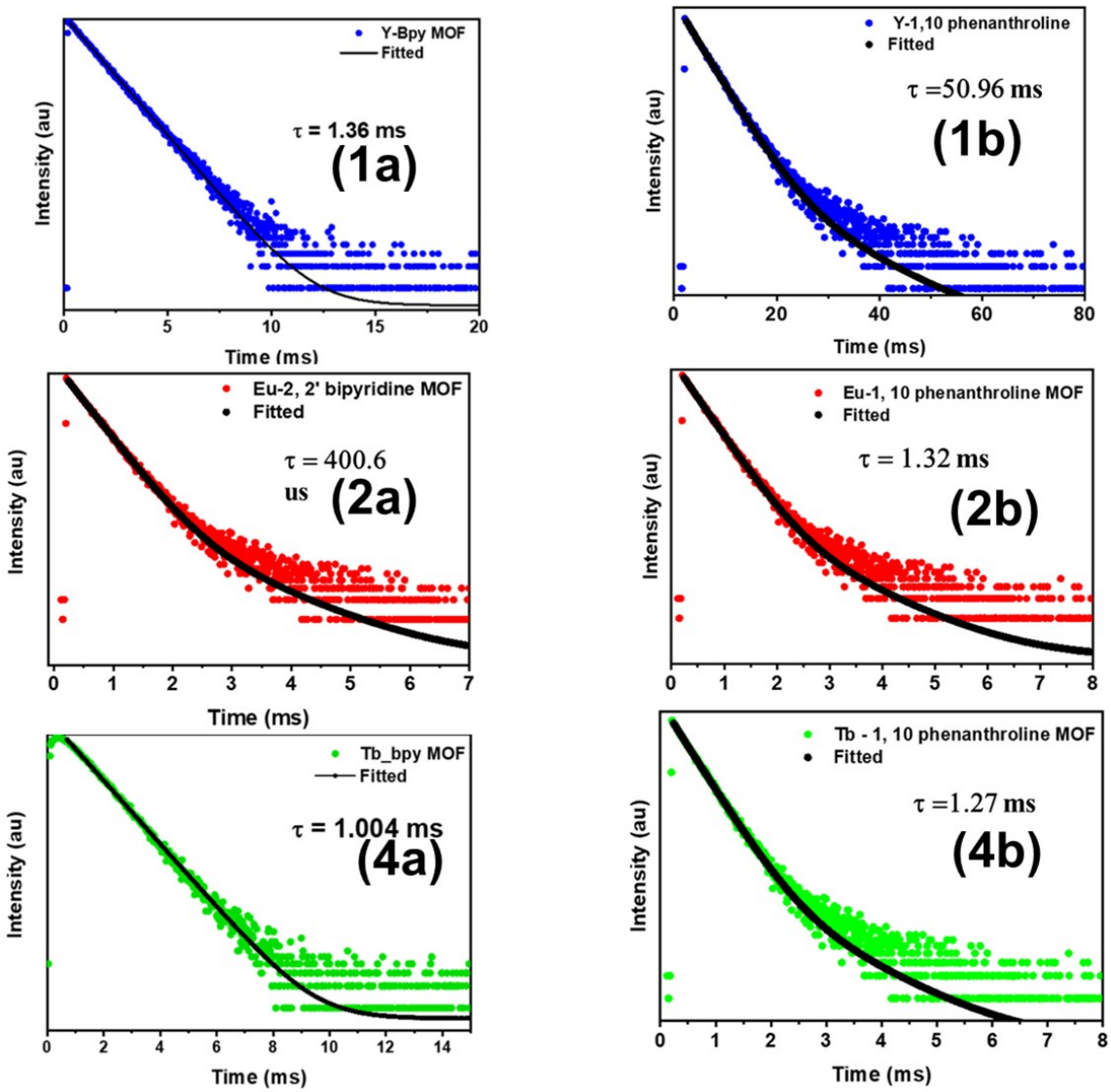

Figure S17. Luminescence decay profiles (298K) for Y, Eu and Tb MOFs.

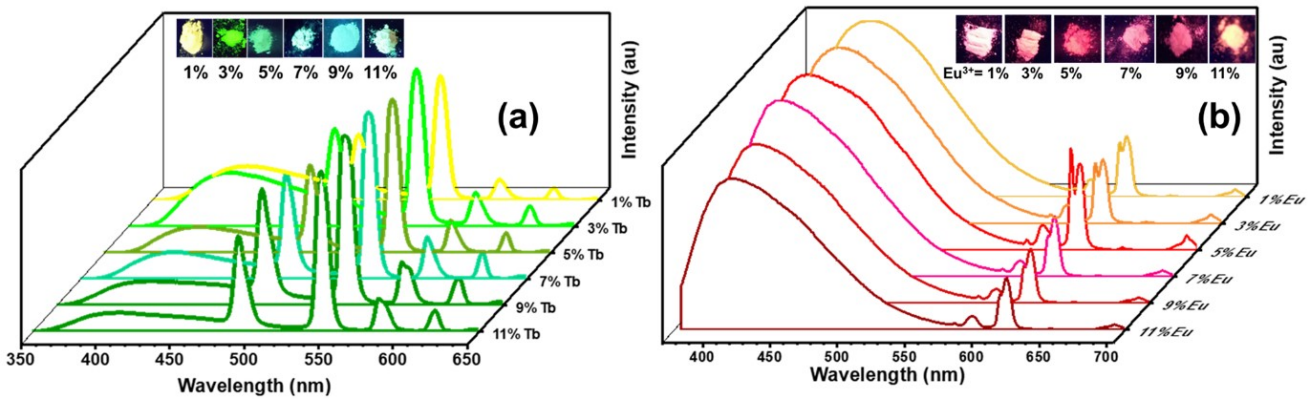

Figure S18. Different substitution of Tb^{3+} **(a)** and Eu^{3+} **(b)** in Y- bpy MOF

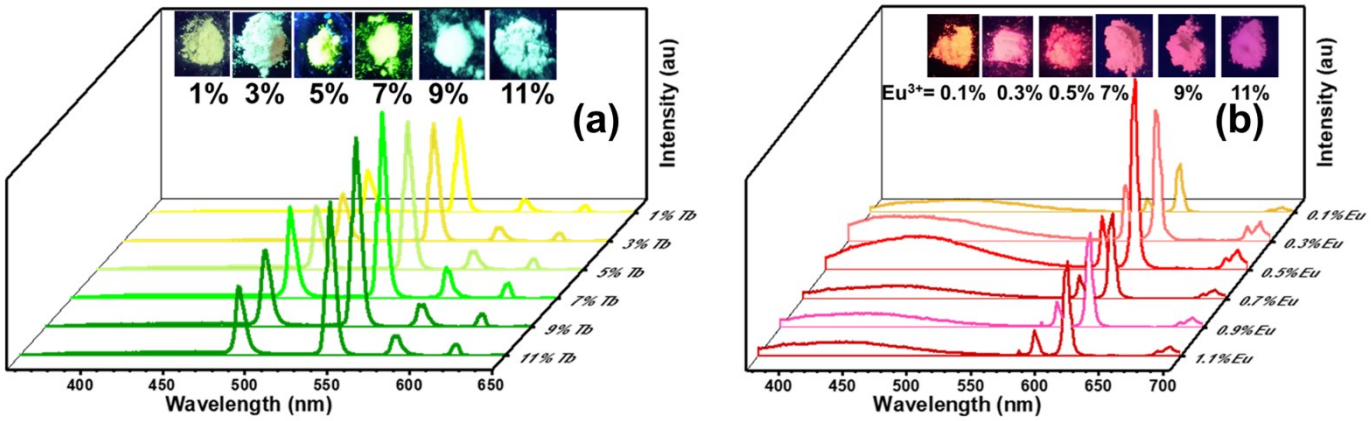

Figure S19. Different substitution of Tb^{3+} **(a)** and Eu^{3+} **(b)** in Y- phen MOF

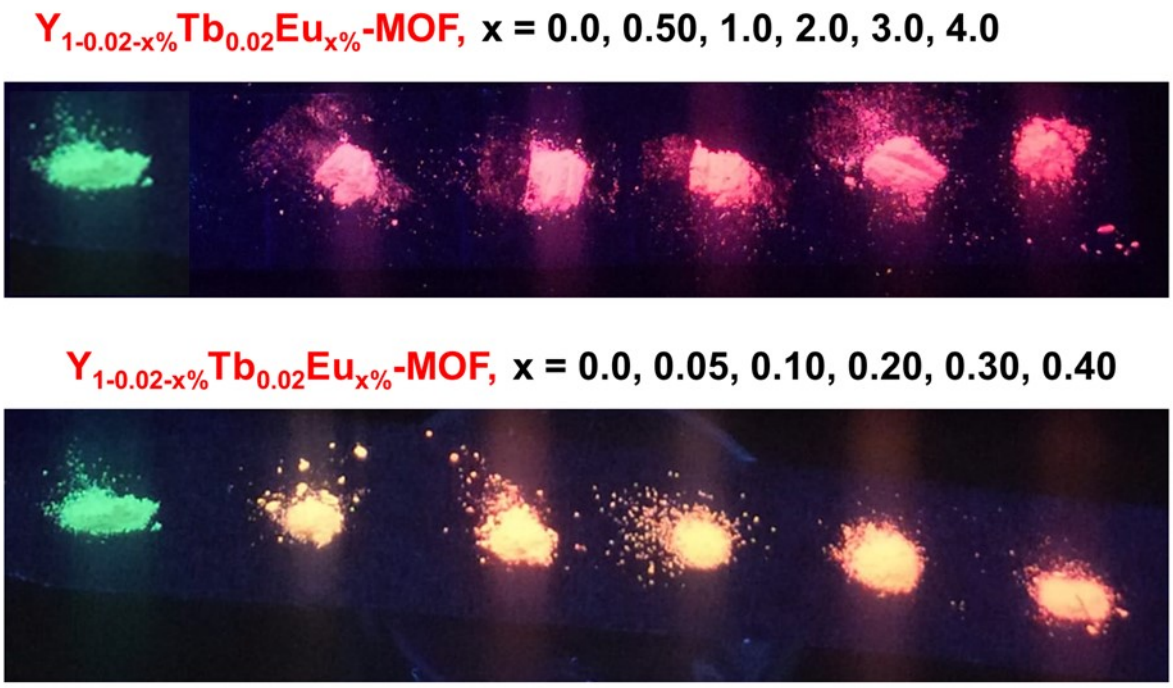

Figure S20. Colour of the $Y_{1-0.02-x\%}Tb_{0.02}Eu_{x\%}$-MOF (x = 0.0, 0.5, 1, 2, 3, 4) and $Y_{1-0.02-0\%}Tb_{0.02}Eu_{x\%}$-MOF (x = 0.0, 0.05, 0.1, 0.2, 0.3, 0.4) samples under UV light

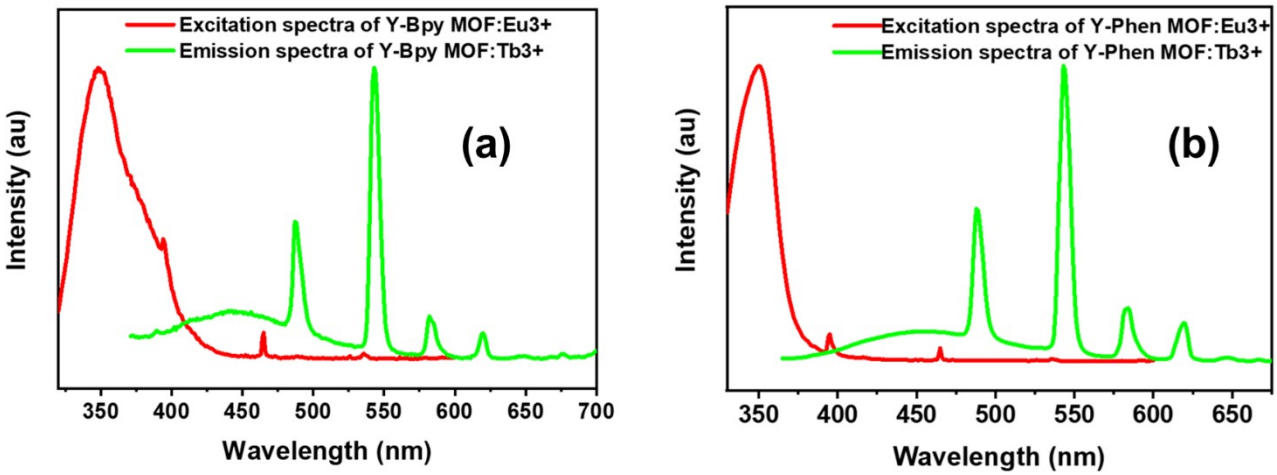

Figure S21. The spectral overlap between the PLE spectrum of Y-MOF: Eu^{3+} and PL spectrum of Y-MOF: Tb^{3+} materials **(a)** Y-bipyridine MOFs **(b)** Y-phenanthroline MOFs.

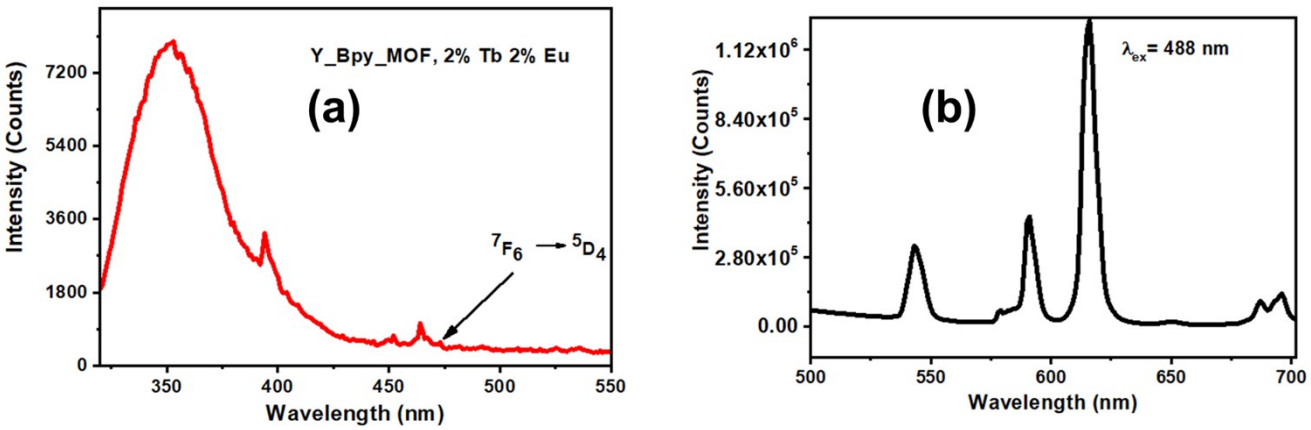

Figure S22. **(a)** The excitation spectrum of Y-MOF bipyridine, 2% Tb^{3+}, 2% Eu^{3+} sample monitored at 616 nm; **(b)** The emission spectrum of the sample at the excitation of 488nm.

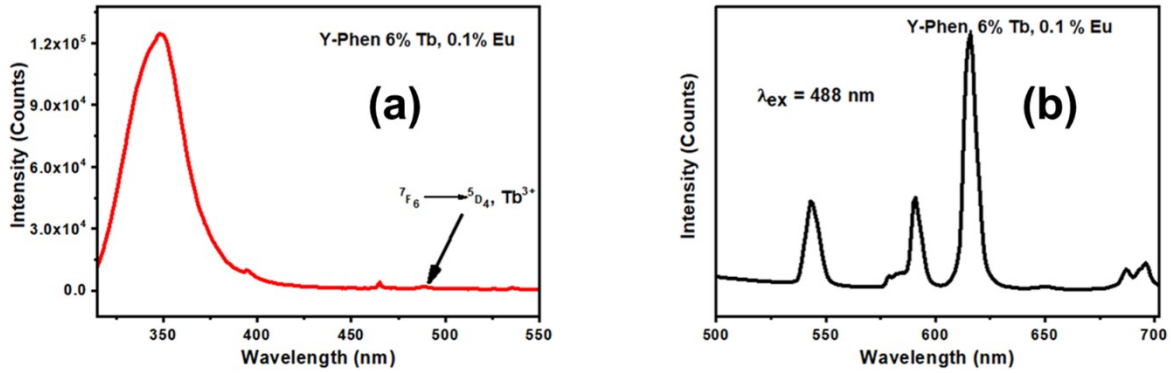

Figure S23. (a) The excitation spectrum of Y-MOF phenanthroline, 6% Tb^{3+}, 0.1% Eu^{3+} sample monitored at 616 nm; **(b)** The emission spectrum of the sample at the excitation of 488 nm.

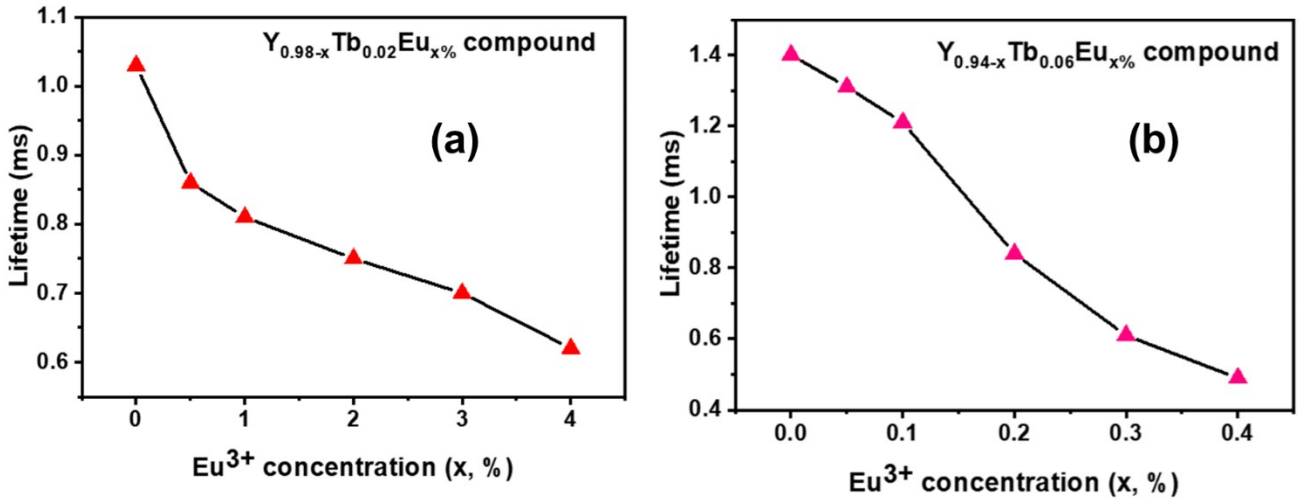

Figure S24. Lifetime vs concentration of the Eu^{3+} plot **(a)** $Y_{0.98-x}Tb_{0.02}Eu_x$ and **(b)** $Y_{0.94-x}Tb_{0.06}Eu_x$ compounds.

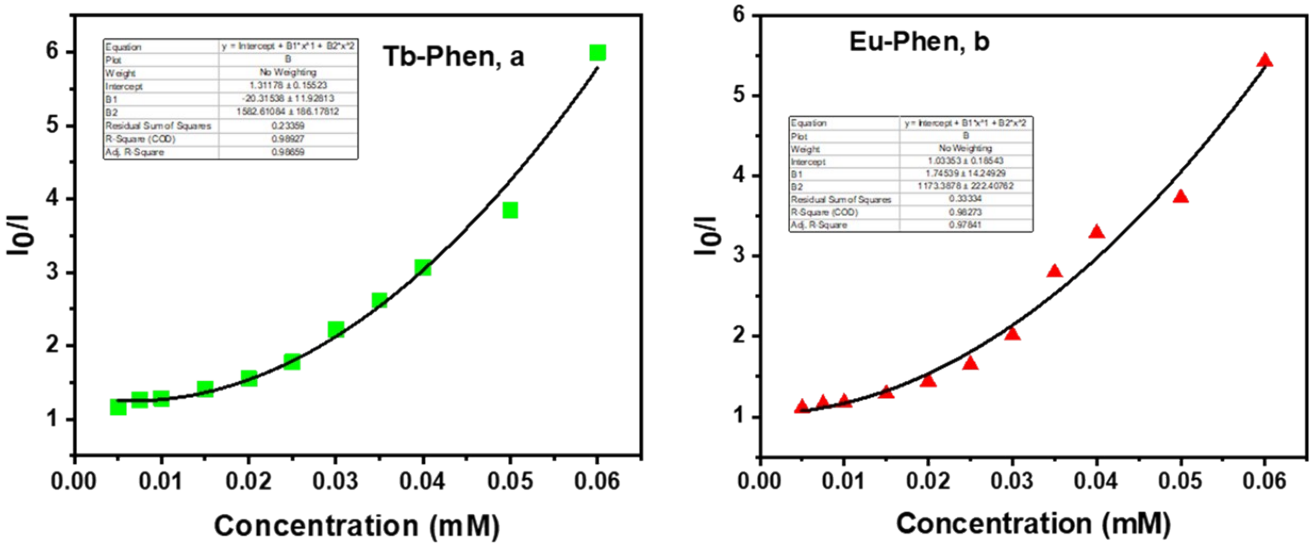

Figure. S25. Stern-Volmer plots for **(a)** Tb and **(b)** Eu – phen MOF at high concentration of azinphos-methyl sensing

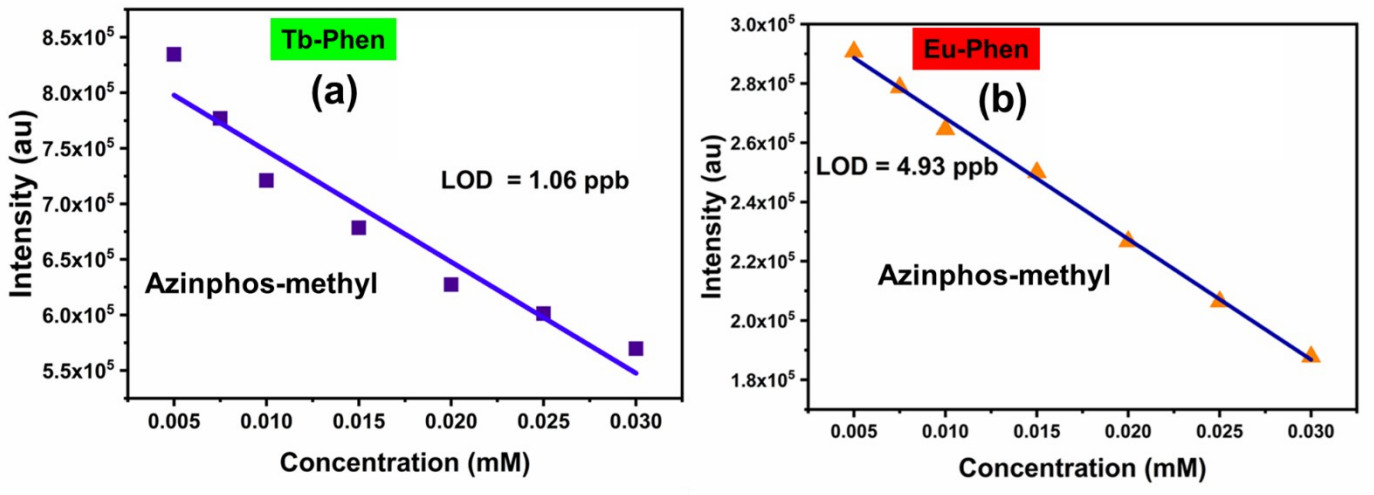

Figure 26. The LOD calculation graph for the pesticide sensing in Tb-phen and Eu-phen MOFs

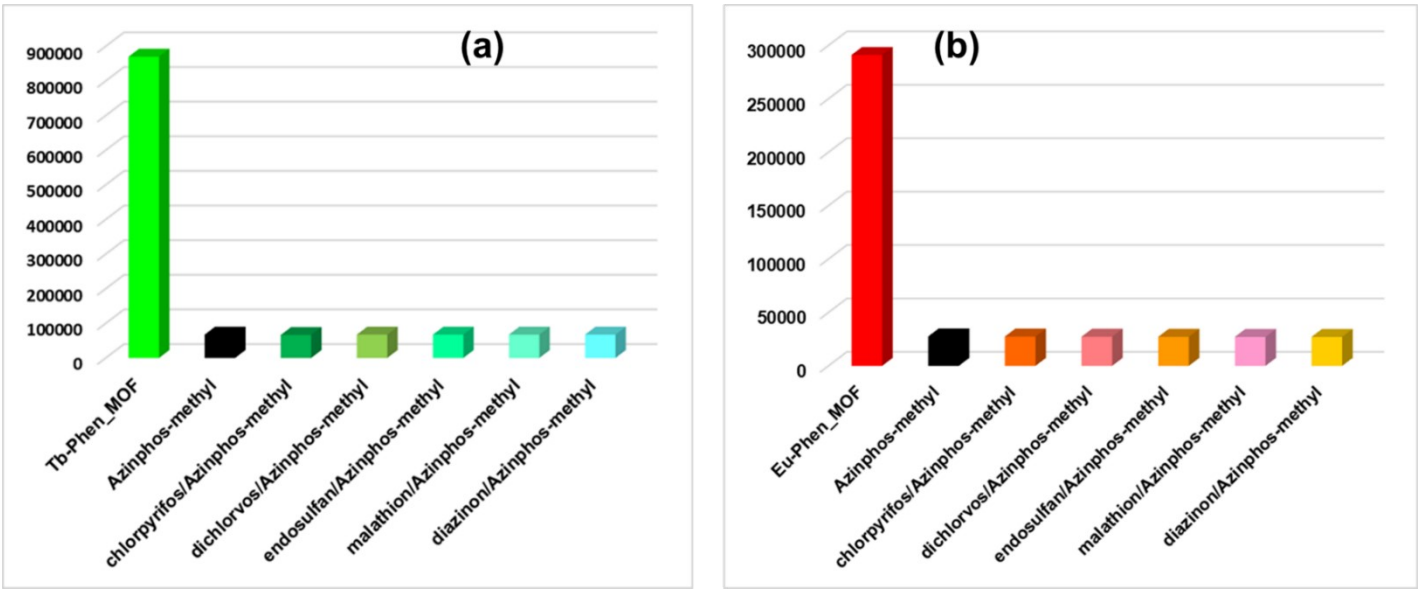

Figure S27. Comparison of the luminescence quenching effect of Azinphos methyl in the presence of other pesticides (75 μM) using **(a)** Tb-phen MOF and **(b)** Eu-phen MOF.

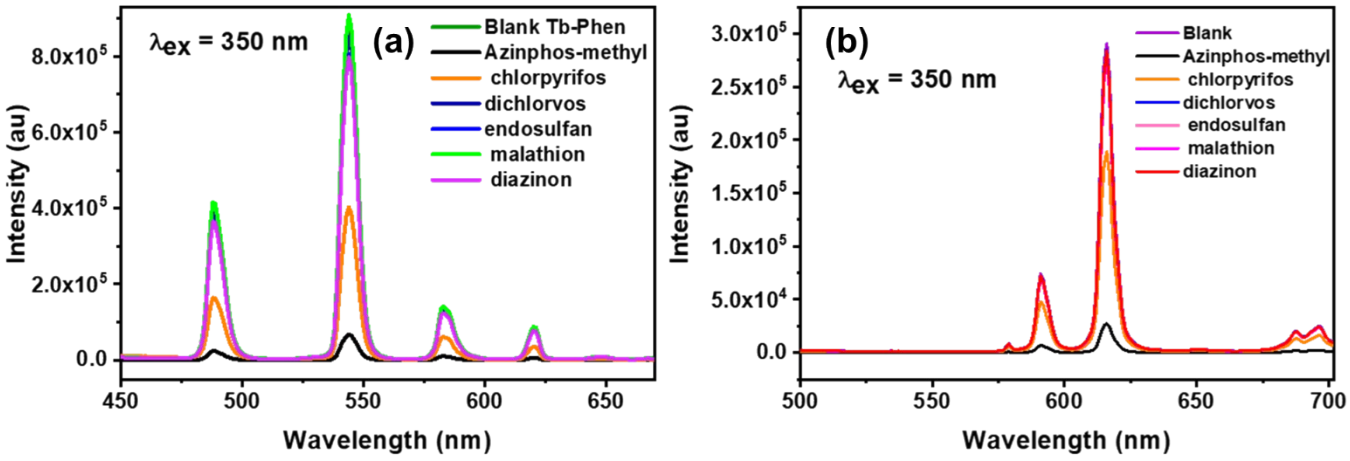

Figure S28. (a) Emission spectra of Tb-phen compound **(b)** Emission spectra of Eu-phen compound dispersed in water upon addition of acetonitrile solution of different pesticide solutions Azinphos-methyl, Chlorpyrivos, Dichlorvos, Endosulfan, Malathion, Diazinon (λ_{ex} = 350 nm). Concentration of pesticides are 75 μM in the medium

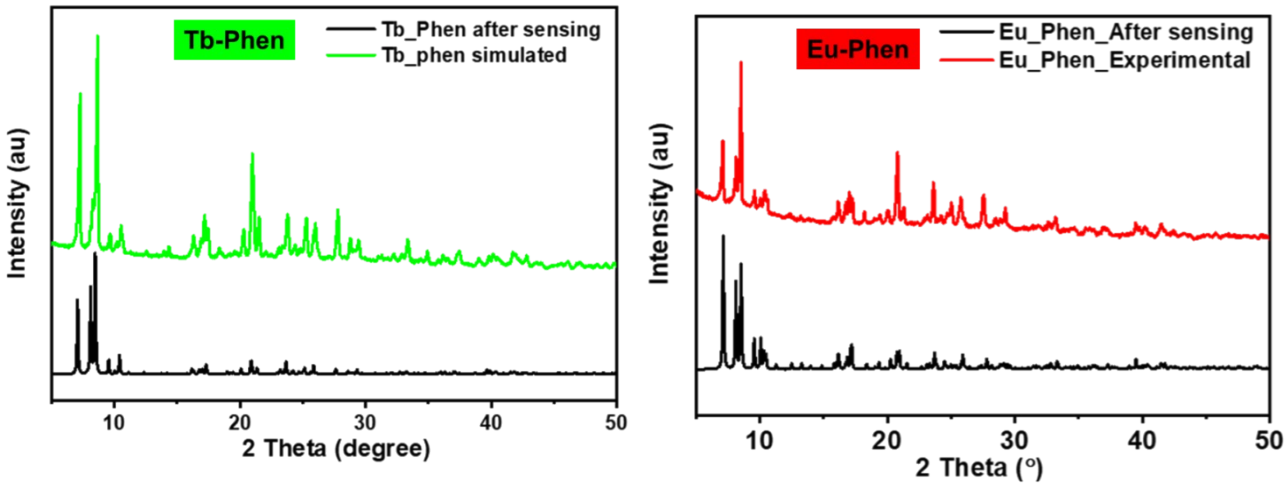

Figure S29. The PXRD study was carried out after the pesticide sensing studies, which indicated the structural integrity of MOF compounds

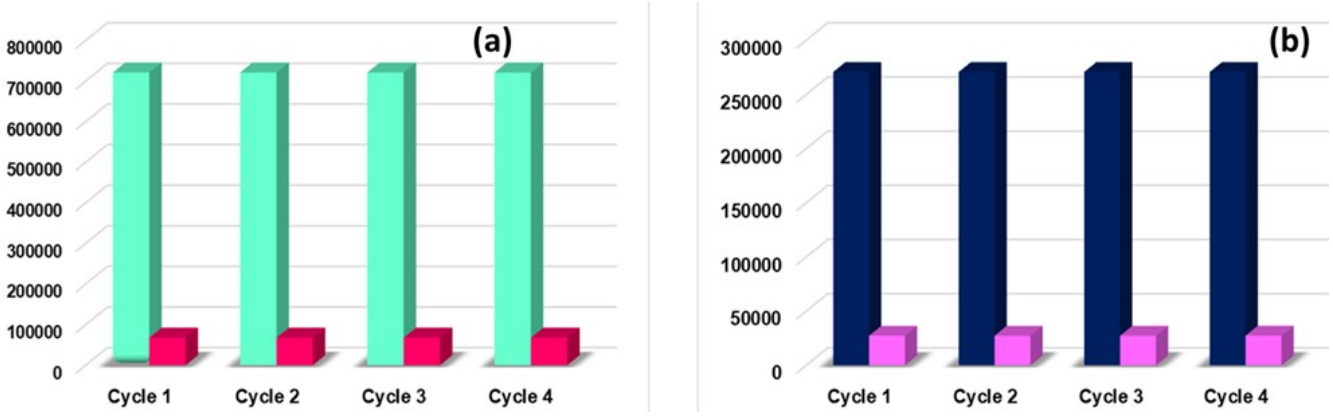

Figure S30. The Recyclability study for the pesticide sensing using the Tb (a) and Eu MOF (b).

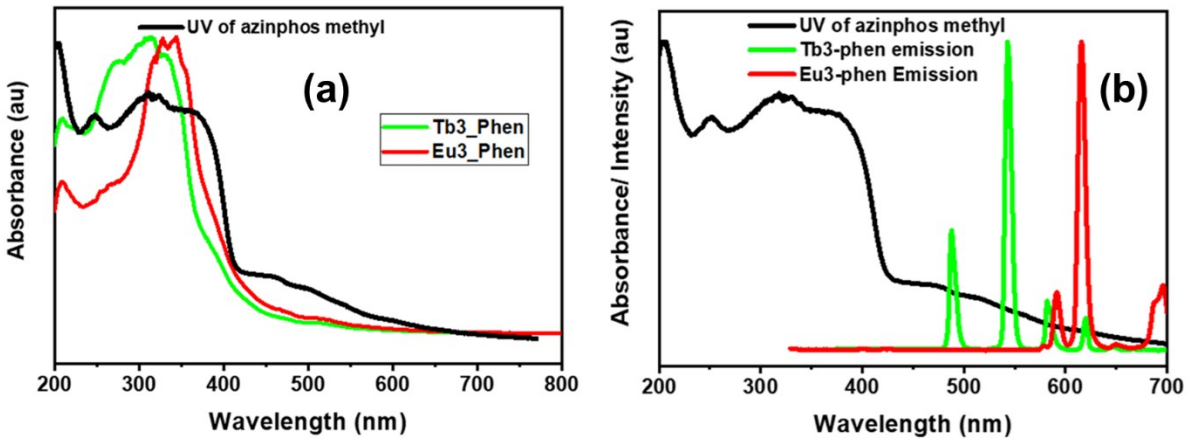

Figure S31. (a) Spectral overlap of the absorption spectra of the azinphos-methyl and the Tb and the Eu – phen MOF compounds. **(b)** The absorption bands of analytes along with the emission spectra of Tb MOF. Note the considerable overlap (see text).

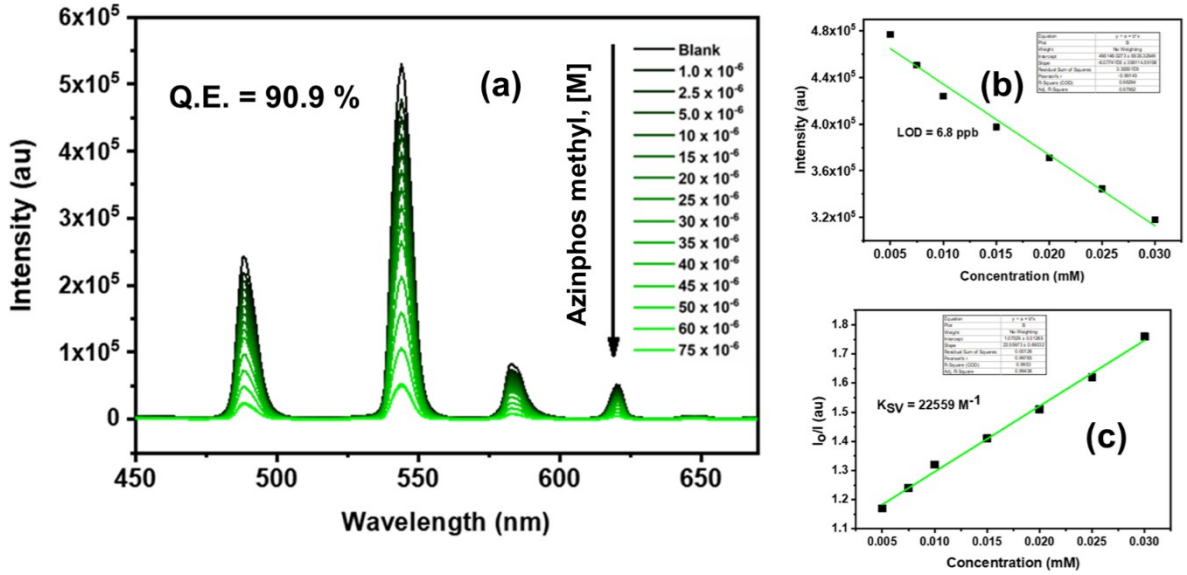

Figure S32. **(a)** Emission spectra of Tb - bpy MOF dispersed in water upon incremental addition of acetonitrile solution of azinphos- methyl (λ_{ex} = 350nm). Final concentration of pesticide in the medium is indicated in the legend. **(b)** The LOD calculation graph for the pesticide sensing in Tb-bpy MOF **(c)** Plot of I_0/I of Tb - bpy MOFs (at 544 nm) *vs* concentration

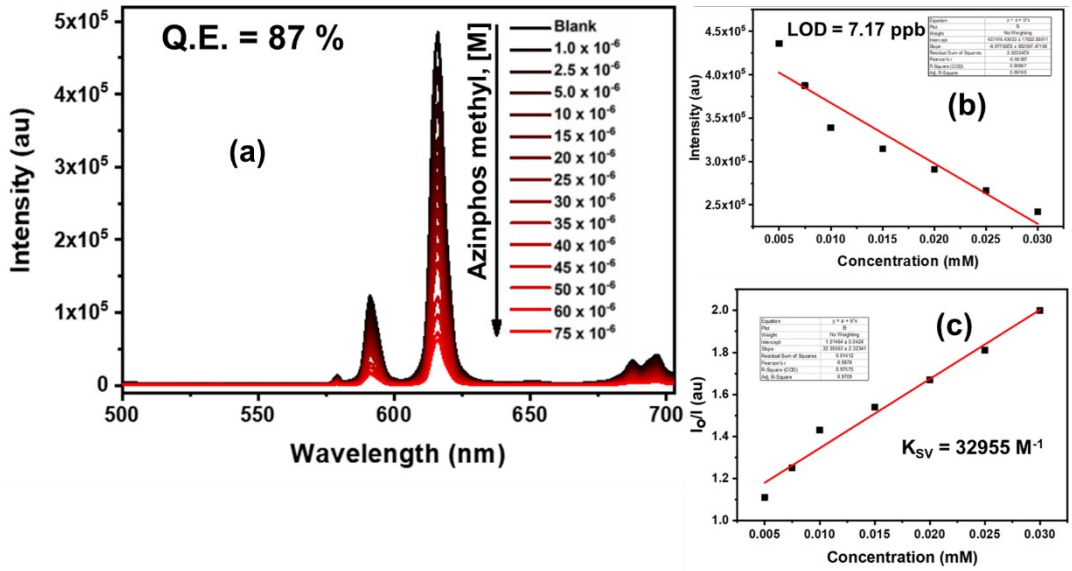

Figure S33. **(a)** Emission spectra of Eu -bpy MOF dispersed in water upon incremental addition of acetonitrile solution of Azinphos - methyl (λ_{ex} = 350nm). Final concentration of pesticide in the medium is indicated in the legend. **(b)** The LOD calculation graph for the

pesticide sensing in Eu-bpy MOF **(c)** Plot of I_0/I of Eu-bpy MOFs (at 616 nm) *vs* concentration

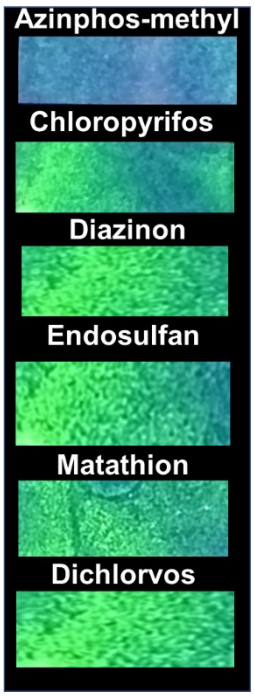

Figure S34. Colour of Tb-phen coated paper strips in presence of different pesticides (75 μM). Note: the green colour vanishes only in the presence of azinphos-methyl.

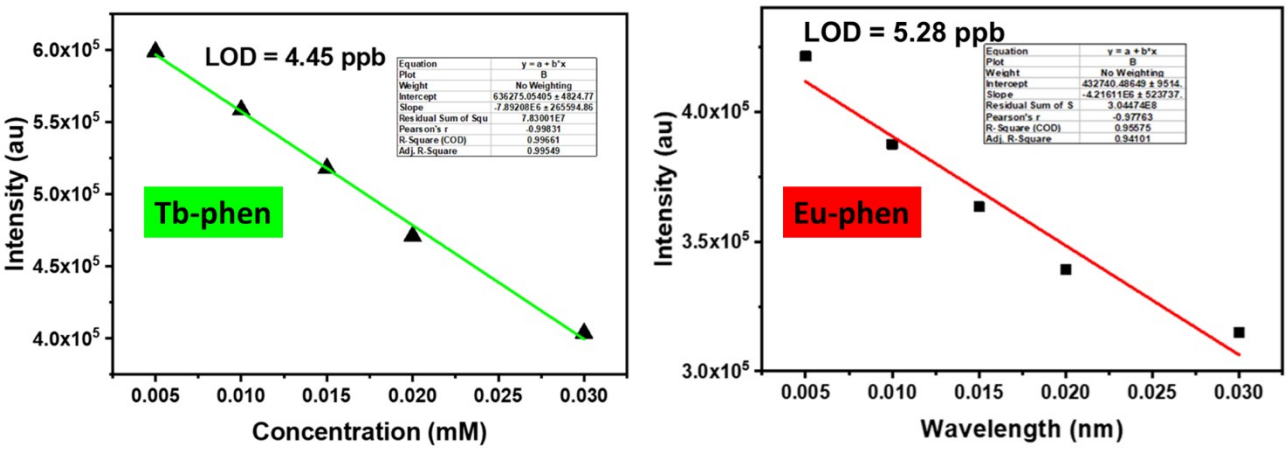

Figure S35. The LOD calculation graph for the azinphos-methyl using paper strips in Tb-phen and Eu-phen

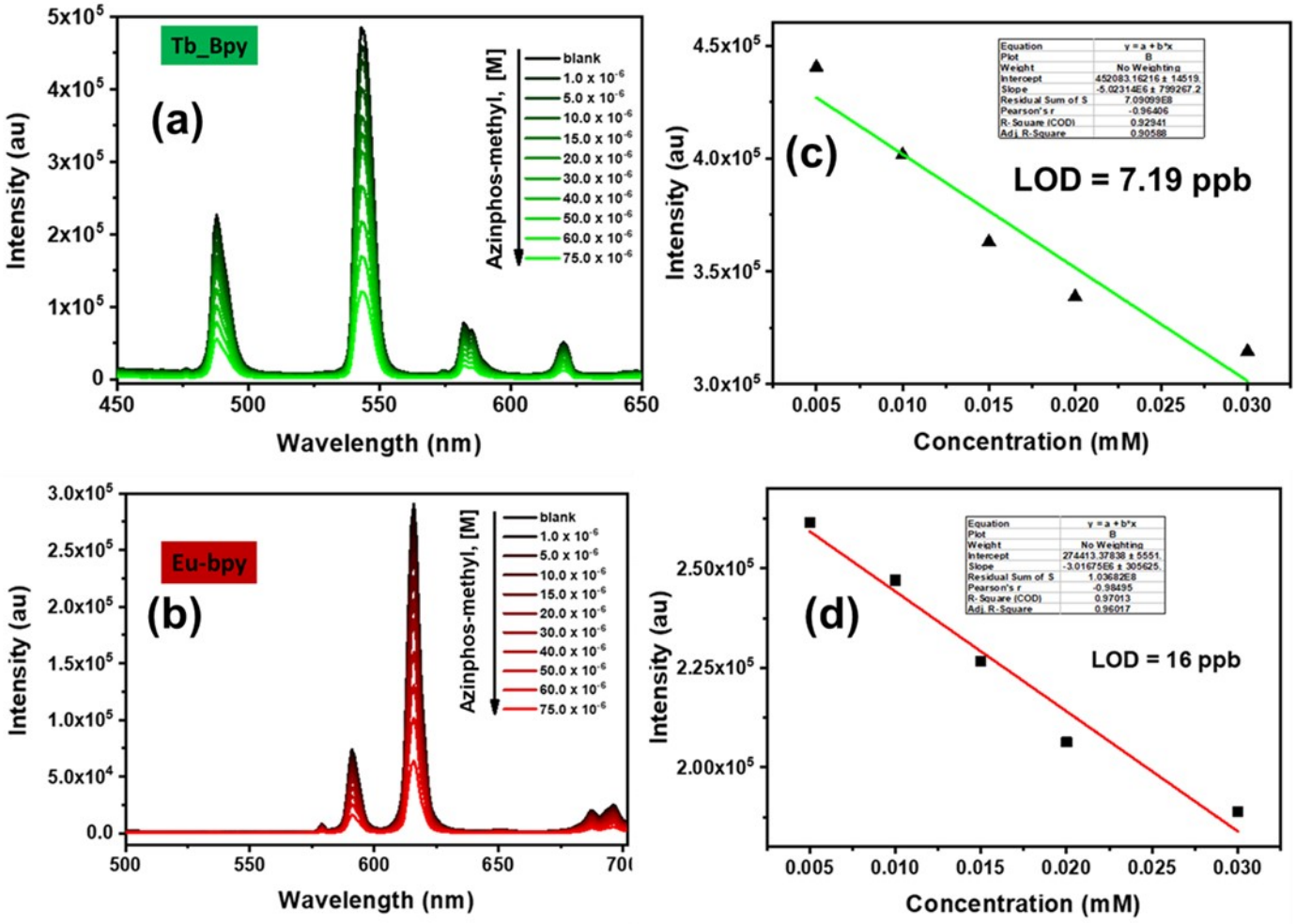

Figure S36. The decrease in luminescence intensity of the MOF coated paper strips dipped in different concentrations of azinphos-methyl solution **(a)** Tb-bpy **(b)** Eu-bpy and LOD values for the azinphos-methyl solution **(c)** Tb-bpy **(d)** Eu-bpy

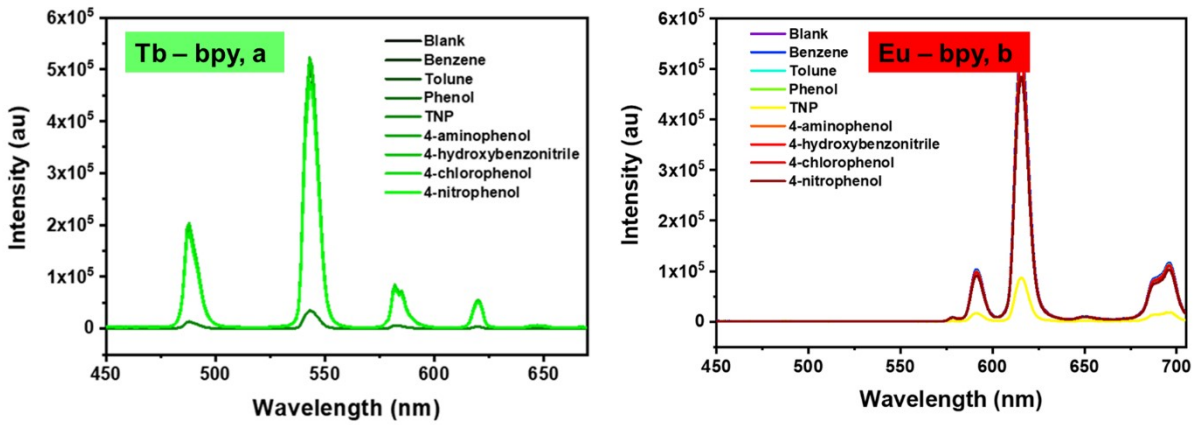

Figure S37. (a) Emission spectra of Tb-bpy compound **(b)** Emission spectra of Eu-bpy compound dispersed in water upon addition of acetonitrile solution of TNP and different Aromatic compound solutions benzene, toluene, phenol (λ_{ex} = 350 nm). Concentration of analytes are 100 μM in the medium

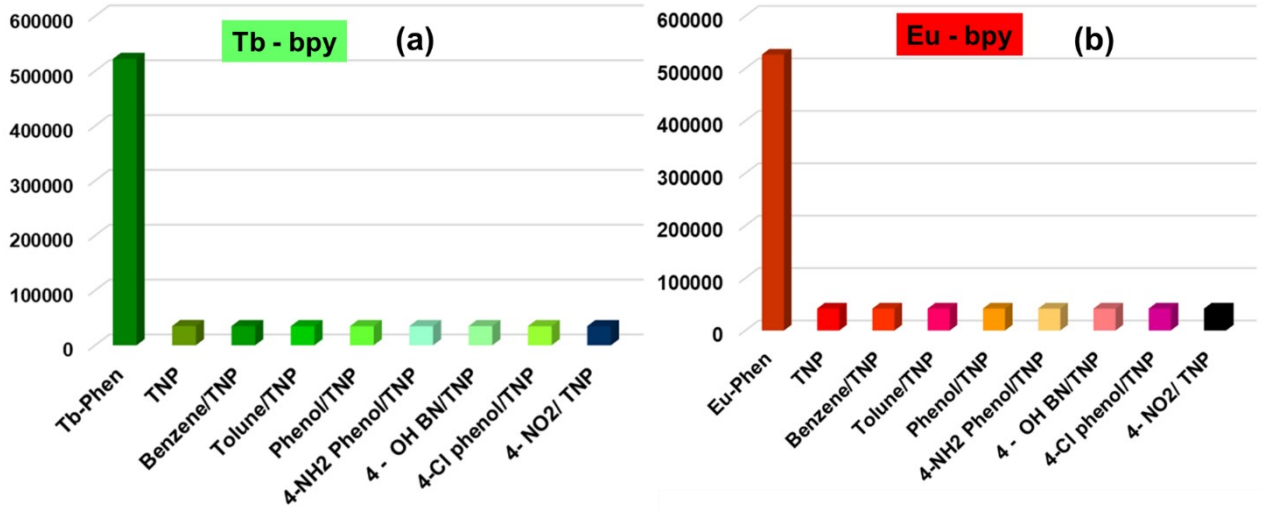

Figure S38. Comparison of the luminescence quenching effect of TNP in the presence of other aromatics (100 μM) using **(a)** Tb-bpy MOF and **(b)** Eu-bpy MOF

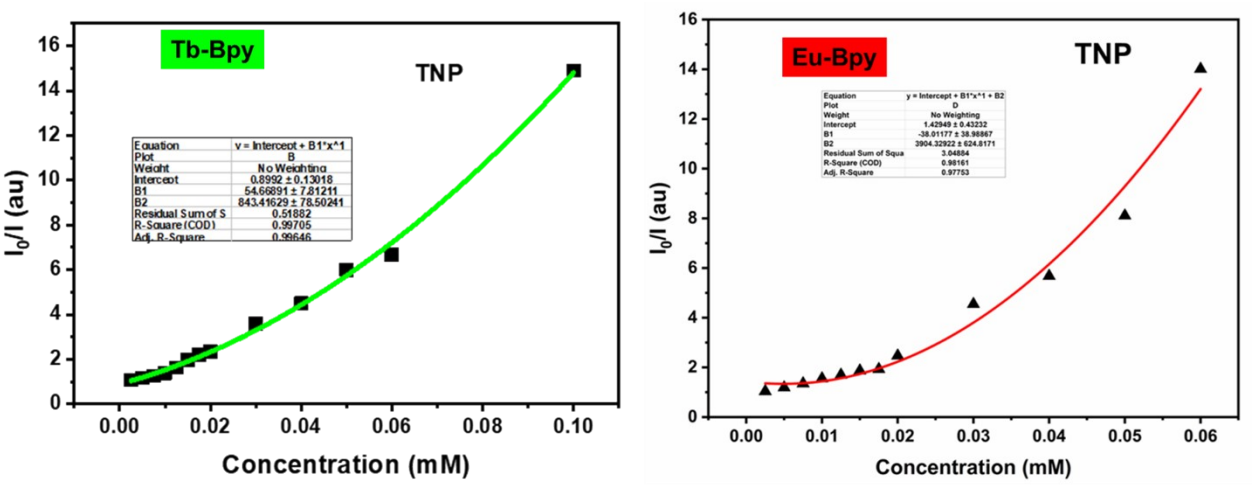

Figure. S39. Stern-Volmer plots for **(a)** Tb and **(b)** Eu – bpy MOFs at high concentration of Trinitrophenol.

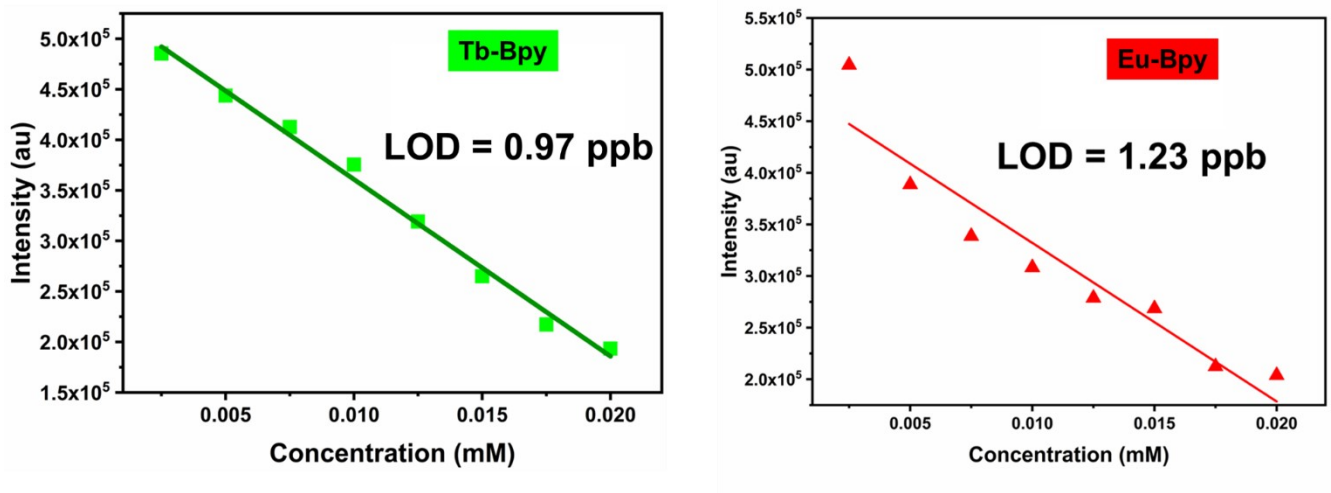

Figure 40. The LOD calculation graph for the TNP sensing in Tb-bpy and Eu bpy

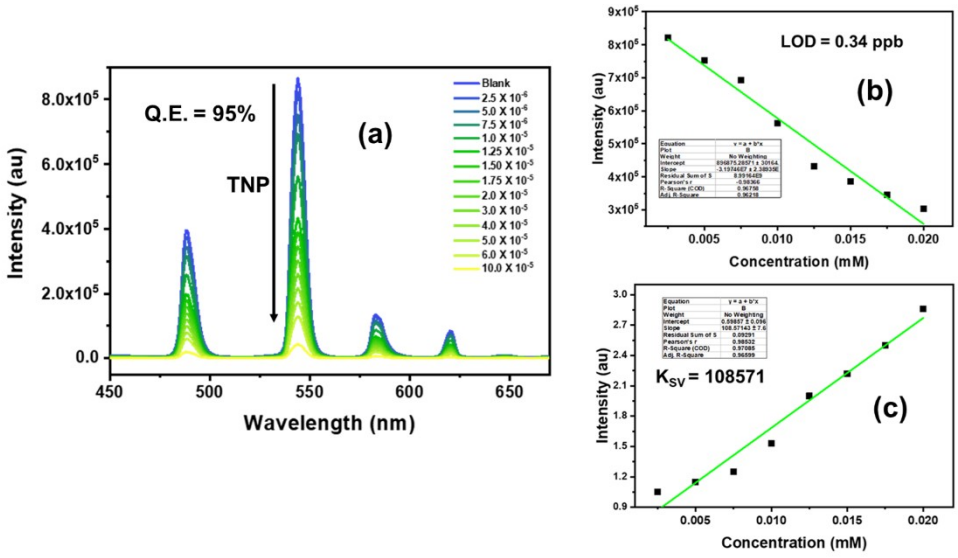

Figure S41. **(a)** Emission spectra of Tb-phen MOF dispersed in water upon incremental addition of acetonitrile solution of Trinitrophenol (λ_{ex} = 350nm). Final concentration of TNP in the medium is indicated in the legend. **(b)** The LOD calculation graph for the TNP sensing in Tb-phen MOF **(c)** Plot of I_0/I of Tb-phen MOF (at 544 nm) *vs* concentration

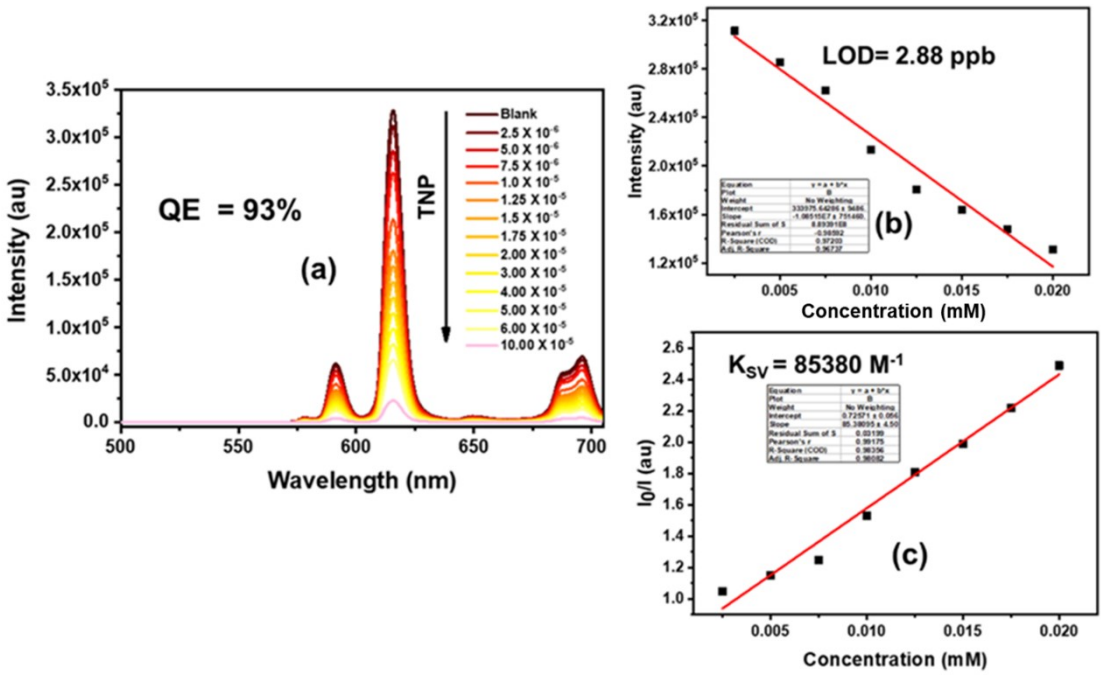

Figure S42. (a) Emission spectra of Eu -phen MOF dispersed in water upon incremental addition of acetonitrile solution of trinitrophenol (λ_{ex} = 350nm). Final concentration of TNP in the medium is indicated in the legend. **(b)** The LOD calculation graph for the TNP sensing in Eu - phen MOF **(c)** Plot of I_0/I of Eu-bpy MOFs (at 616 nm) *vs* concentration

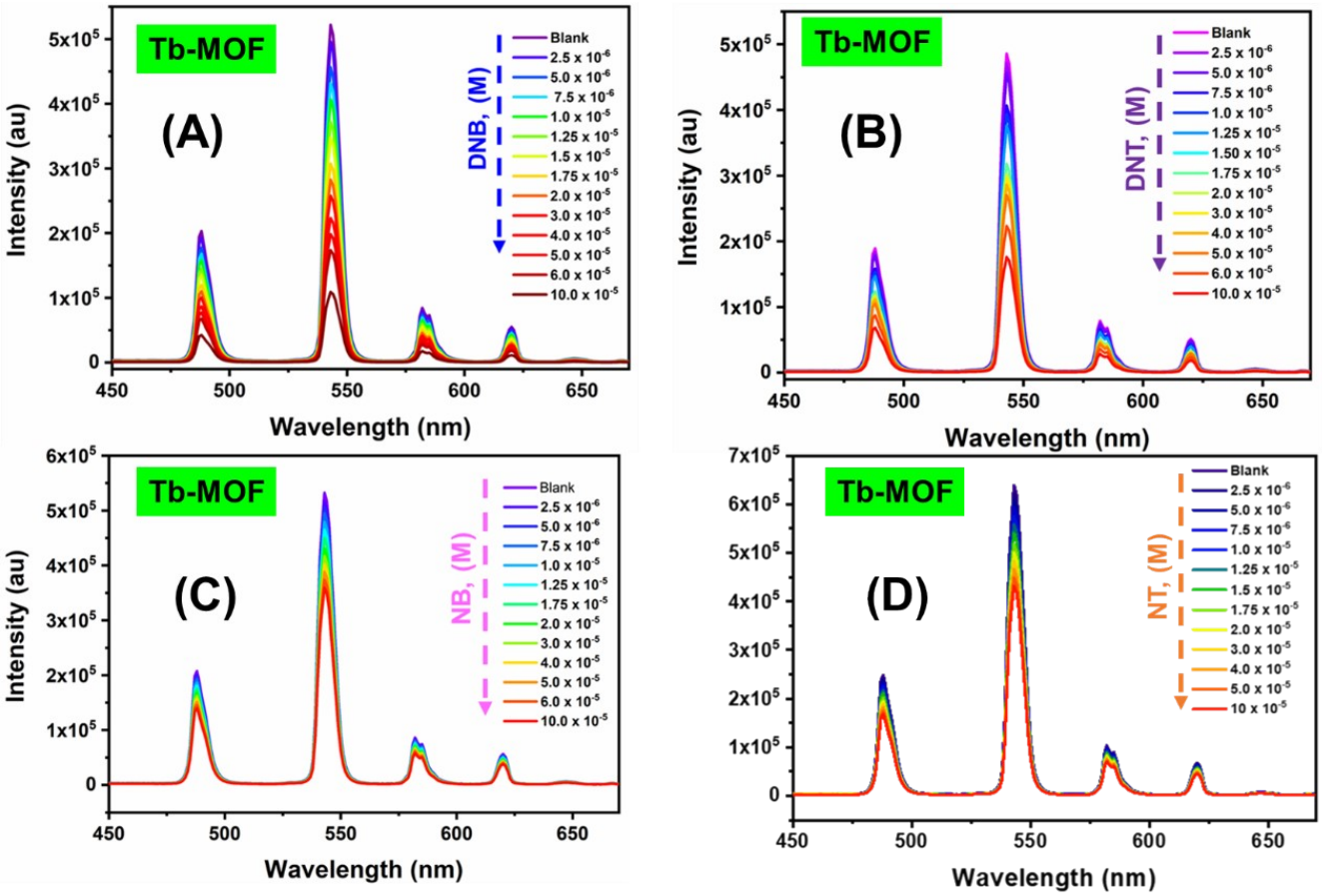

Figure S43. Emission spectra of Tb-bpy MOF dispersed in acetonitrile upon incremental addition of (a) DNB (b) DNT (c) NB (d) NT solution (λex = 350 nm). The final concentration of all the nitroaromatics in the medium is indicated in the legend. The Quenching Efficiency is 77 %, 52.2 %, 32.49 %, 32.28 % respectively.

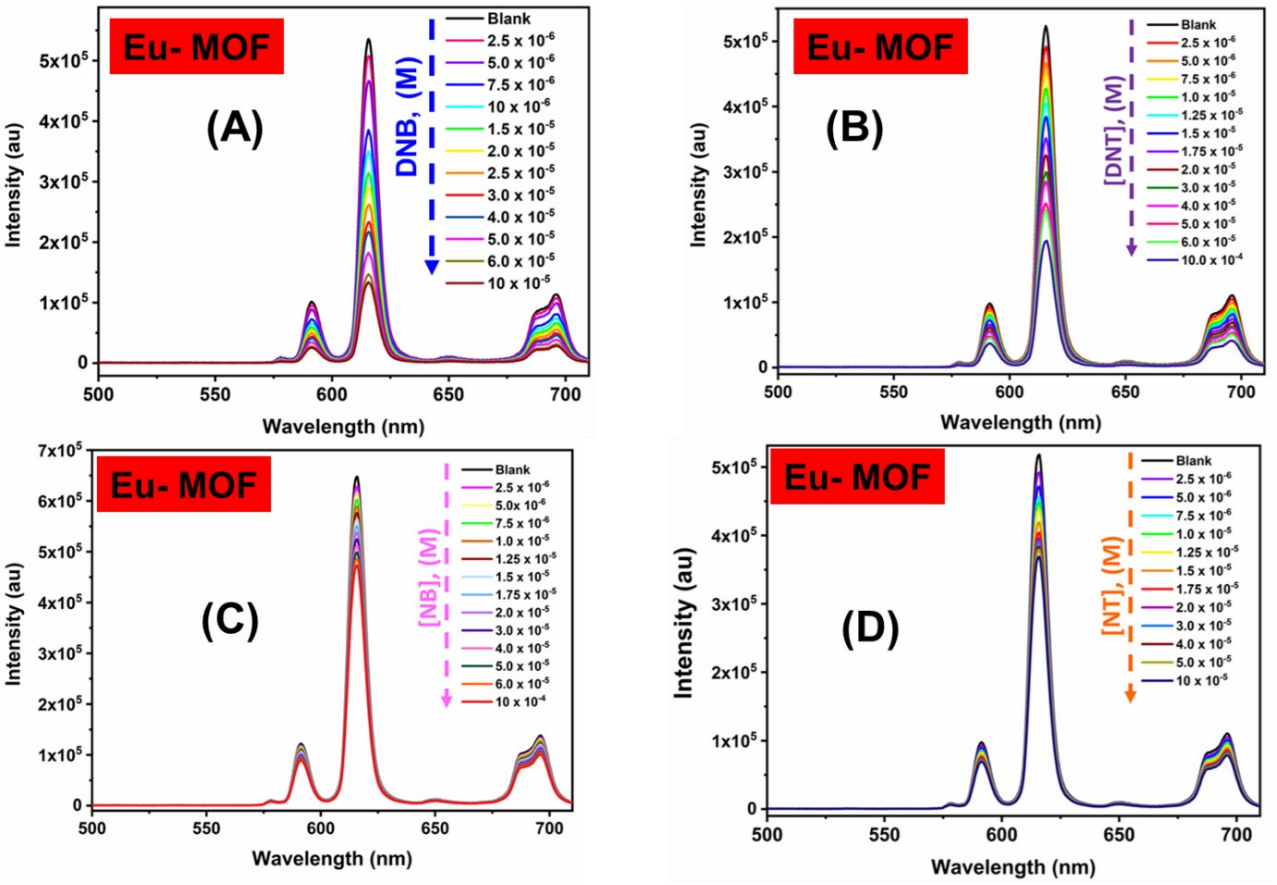

Figure S44. Emission spectra of Eu-bpy MOF dispersed in acetonitrile upon incremental addition of (a) DNB (b) DNT (c) NB (d) NT solution (λex = 350 nm). The final concentration of all the nitroaromatics in the medium is indicated in the legend. The Quenching Efficiency is 75 %, 63.5 %, 28.68 %, 27.62 % respectively.

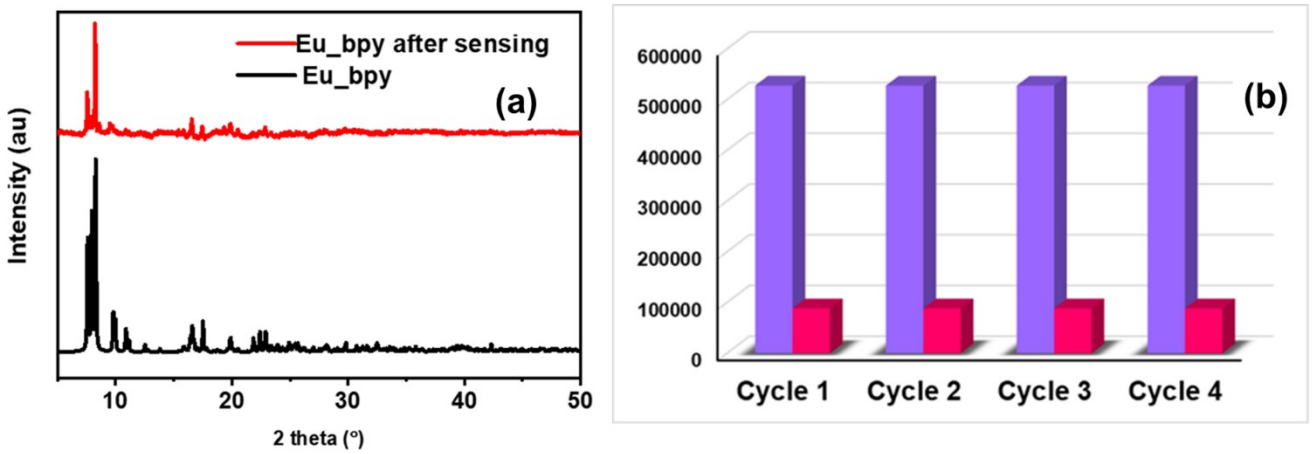

Figure S45. The structural retention of the Eu – bpy MOF after nitroaromatic sensing (a) and recyclability study for the nitroaromatic sensing using the Eu MOF (b).

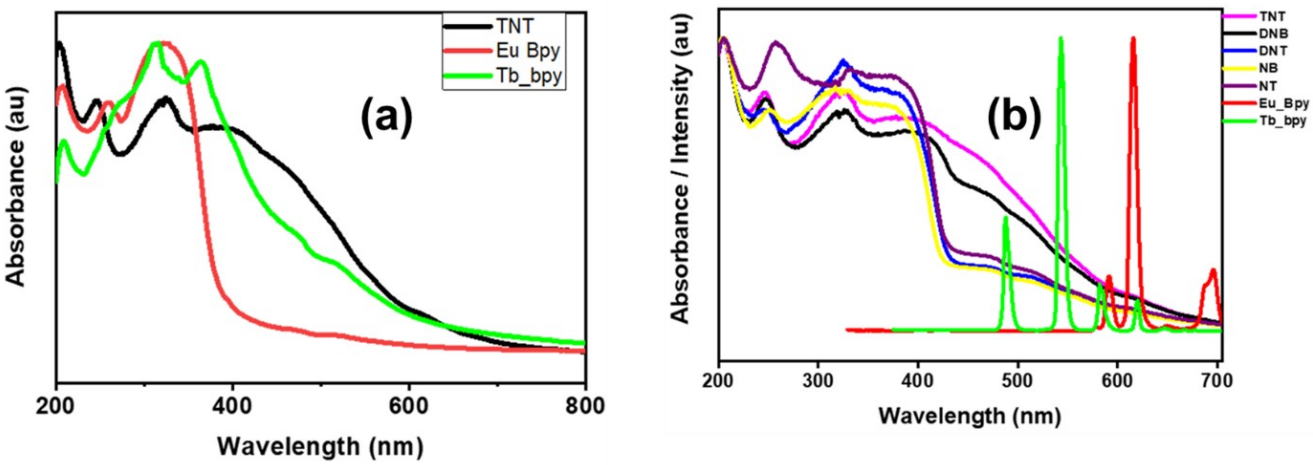

Figure S46. (a) Spectral overlap of the absorption spectra of the trinitrotoluene and the Tb and the Eu – bpy MOF compounds. **(b)** The absorption bands of analytes along with the emission spectra of Eu and Tb MOF. Note the considerable overlap (see text).

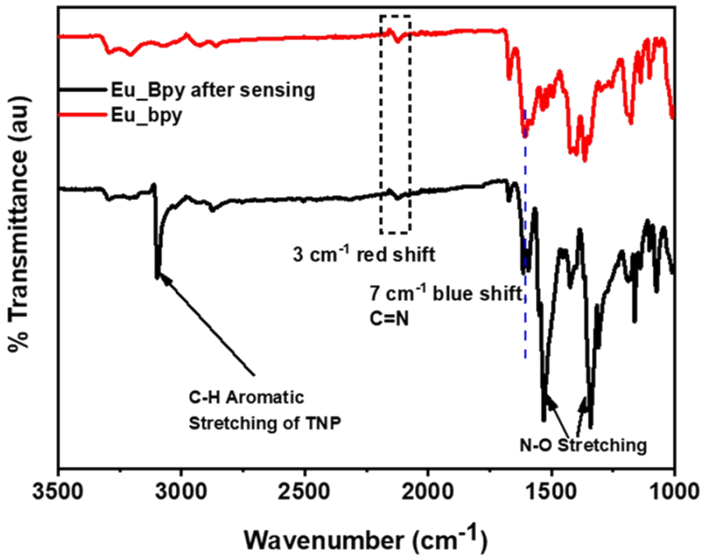

Figure S47. IR spectra of Eu – bpy MOF before and after the pesticide sensing. Note: the shift in the different spectra.

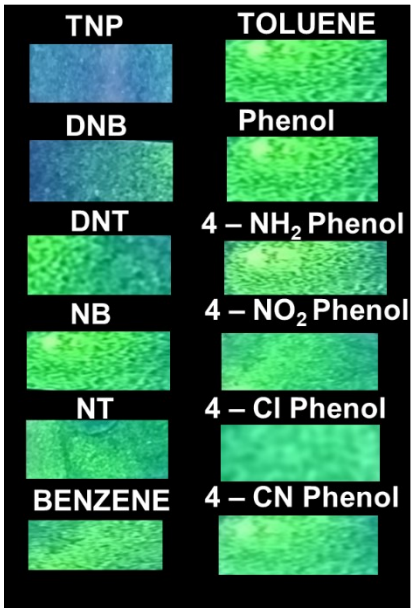

Figure S48. Colour of Tb-bpy coated paper strips in presence of different aromatics. Note: the green colour vanishes only in the presence of TNP

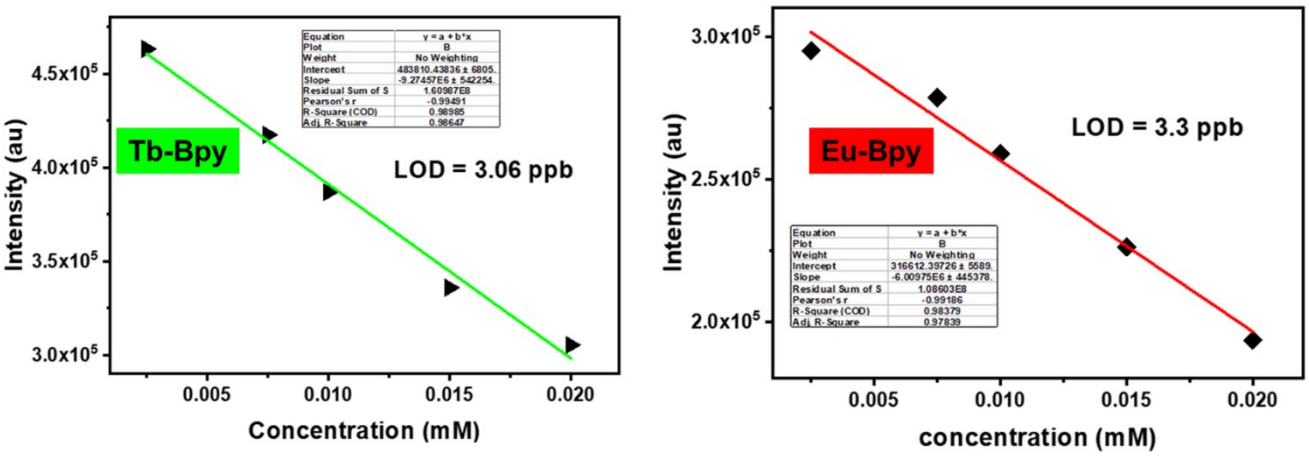

Figure S49: The LOD calculation graph for the TNP using paper strips in Tb-bpy and Eu-bpy.

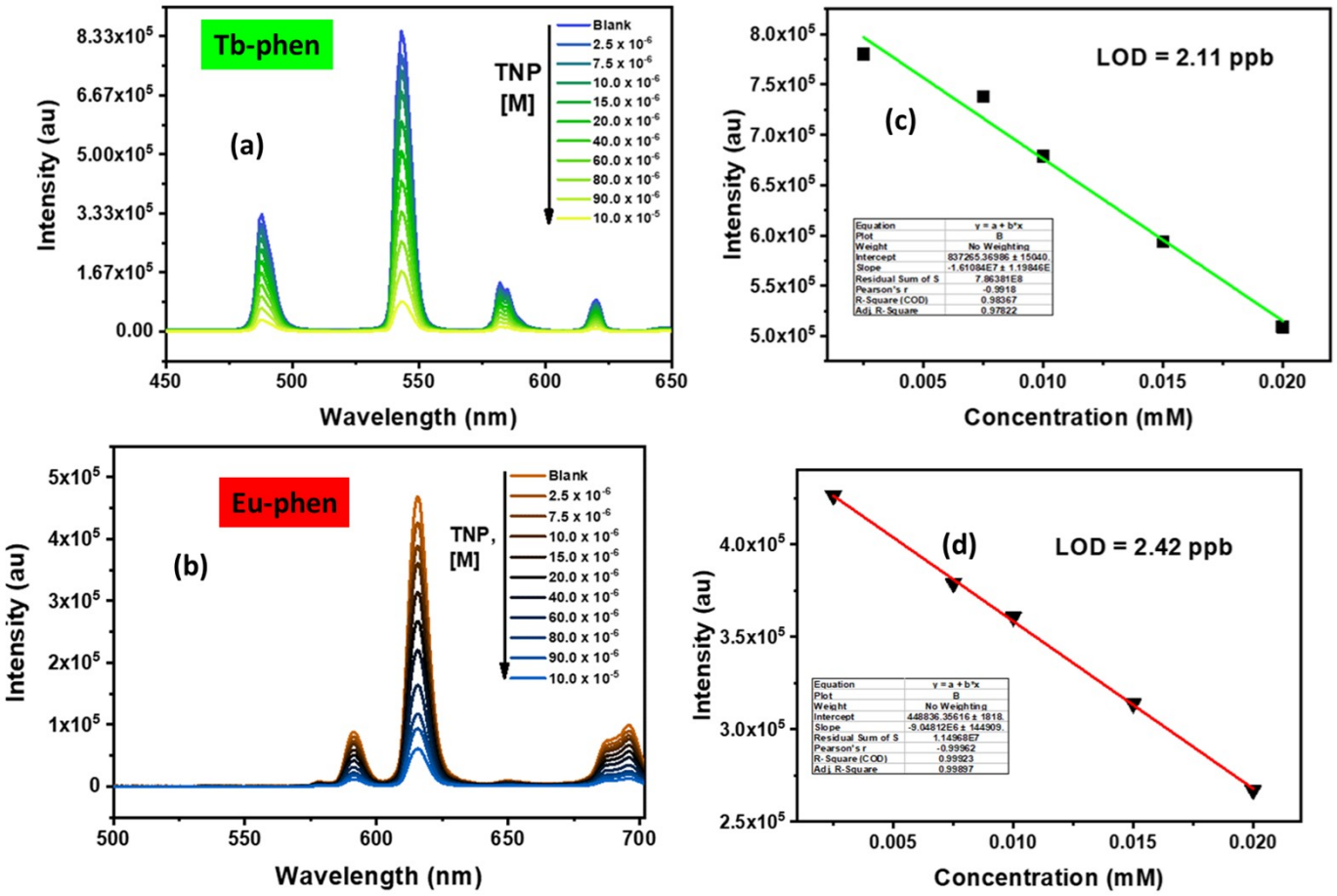

Figure S50: The decrease in luminescence intensity of the MOF coated paper strips dipped in different concentrations of TNP solution **(a)** Tb-phen **(b)** Eu-phen and LOD values for the TNP solution **(c)** Tb- phen **(d)** Eu- phen

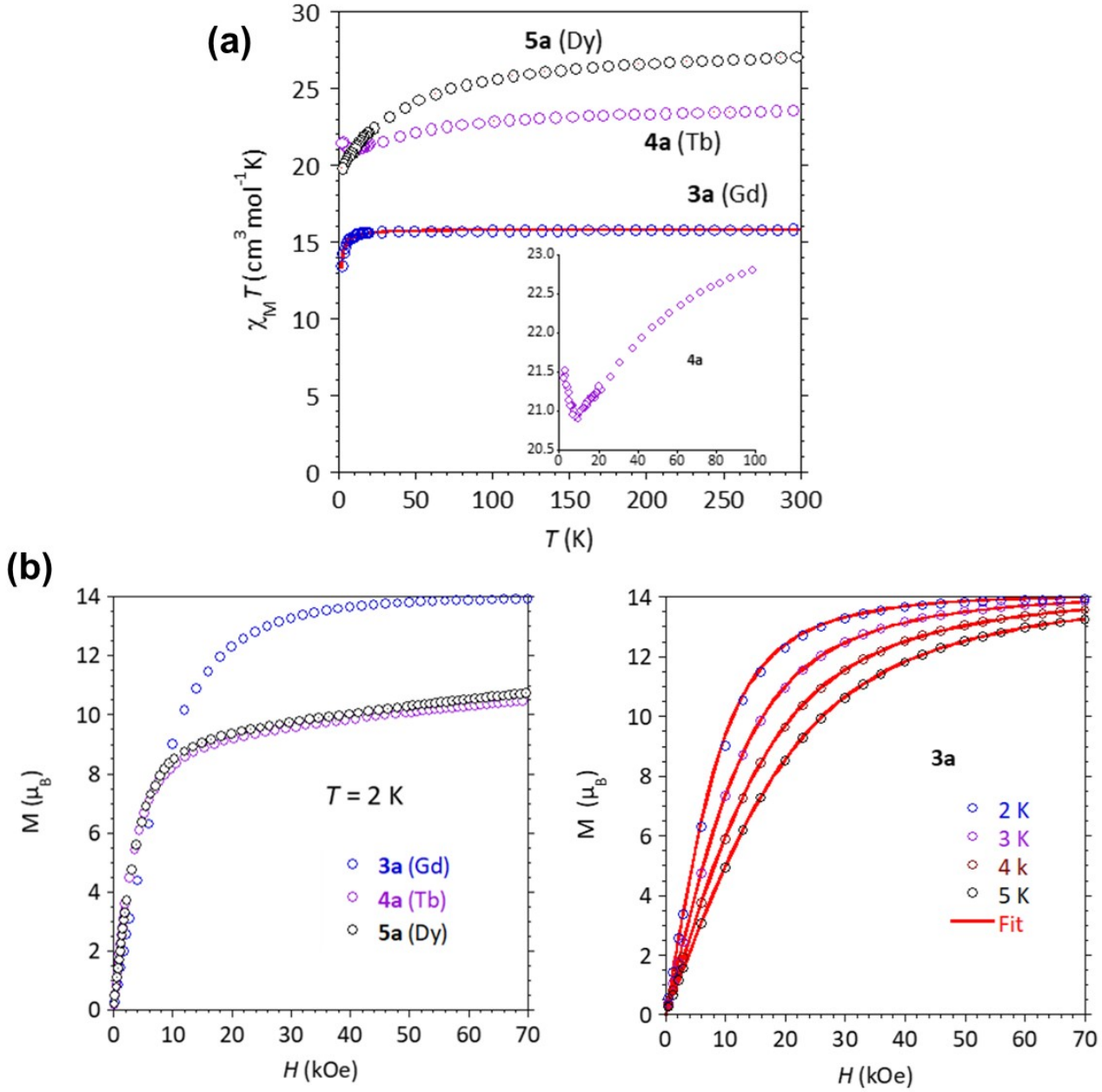

Figure S51. (a) Experimental $\chi_M T$ versus T and (b) M versus H behaviors for **3a**, **4a**, **5a**. The insert in (a) is the low temperature behavior for the Tb derivative. The full line is the calculated behavior for the Gd compound with best-fit parameters J_{GdGd} = -0.041 +/- 0.001 cm^{-1}, g = 2.00 ($H = -J\mathbf{S}_{Gd1}.\mathbf{S}_{Gd2}$).

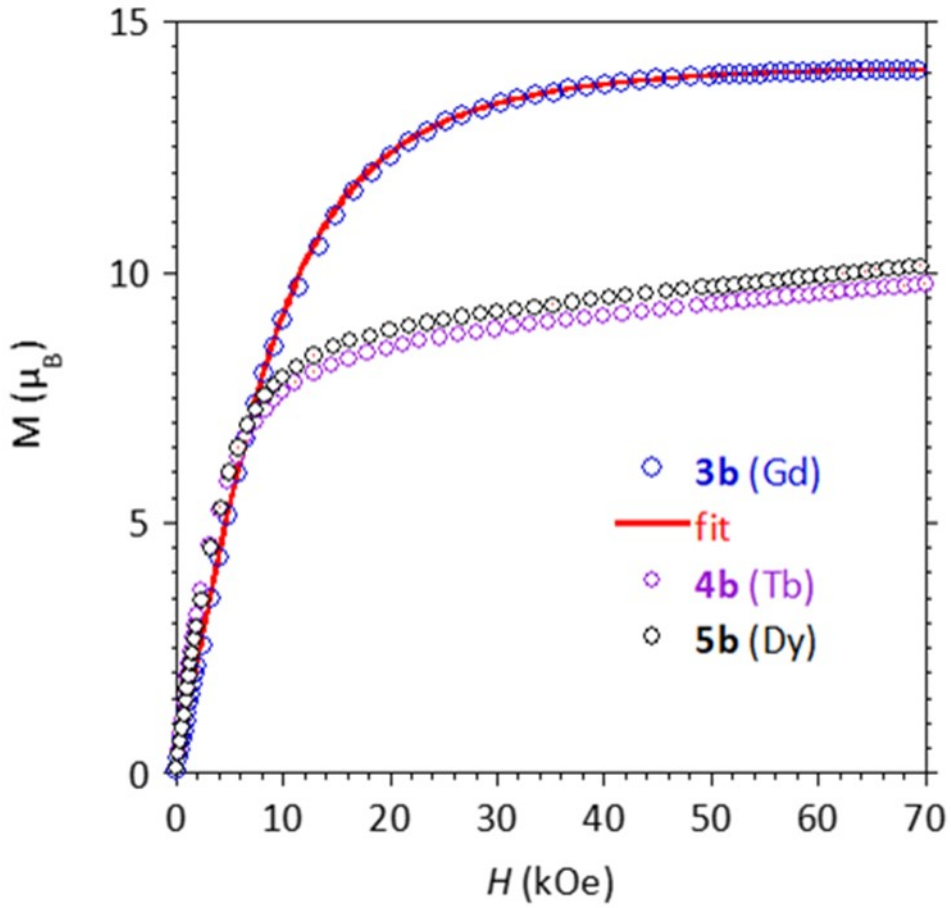

Figure S52. Field dependence of the magnetization of 3b, 4b, and 5b recorded at 2 K.

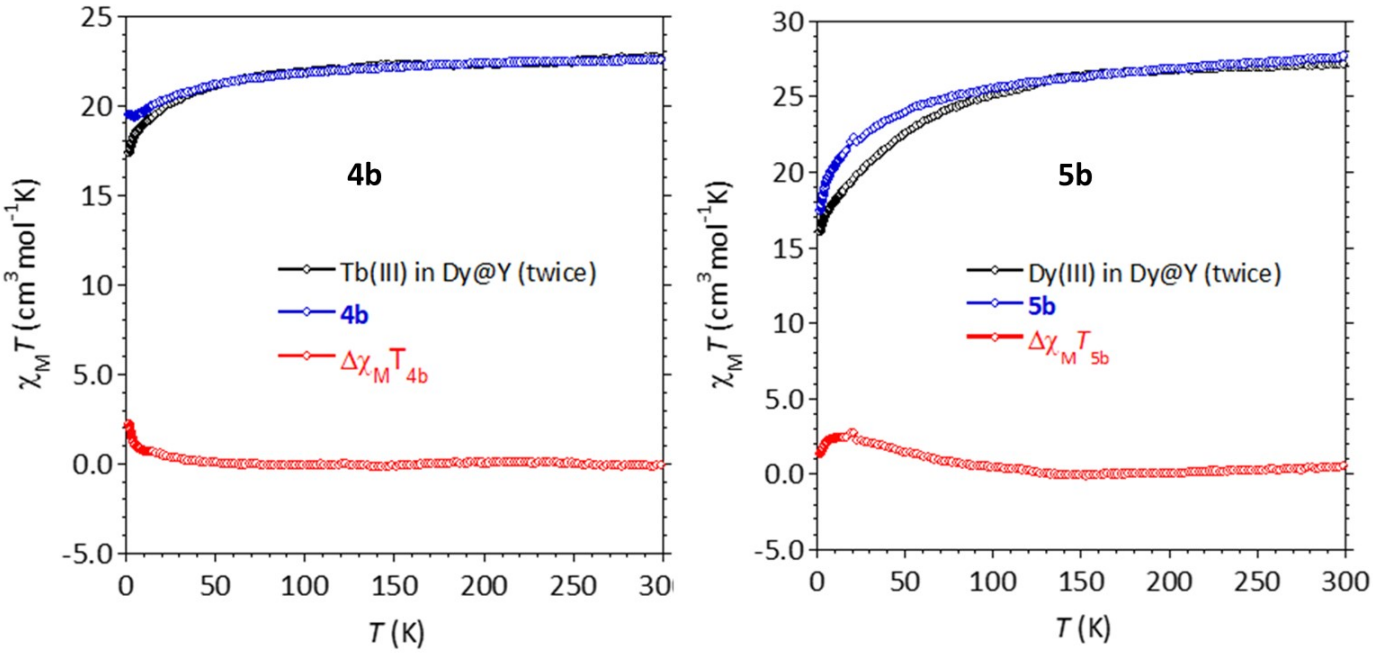

Figure S53. Qualitative Comparison of the $\chi_M T$ versus T behaviors for (a) **4b** and (b) **5b** with the behaviors for isolated Tb(III) and Dy(III) in homologous Y-MOF revealing the contribution ($\Delta\chi_M T$) of the exchange interaction. The contribution of the exchange interaction ($\Delta\chi_M T$ in the plots) was obtained by subtraction the intrinsic magnetic behavior of two isolated Ln ions (i.e. 2× $\chi_M T$ of Ln@Y, black trace below) from $\chi_M T$ of **4b** or **5b**.[21–23] The increase of $\Delta\chi_M T$ at low T is indicative for a ferromagnetic interaction.

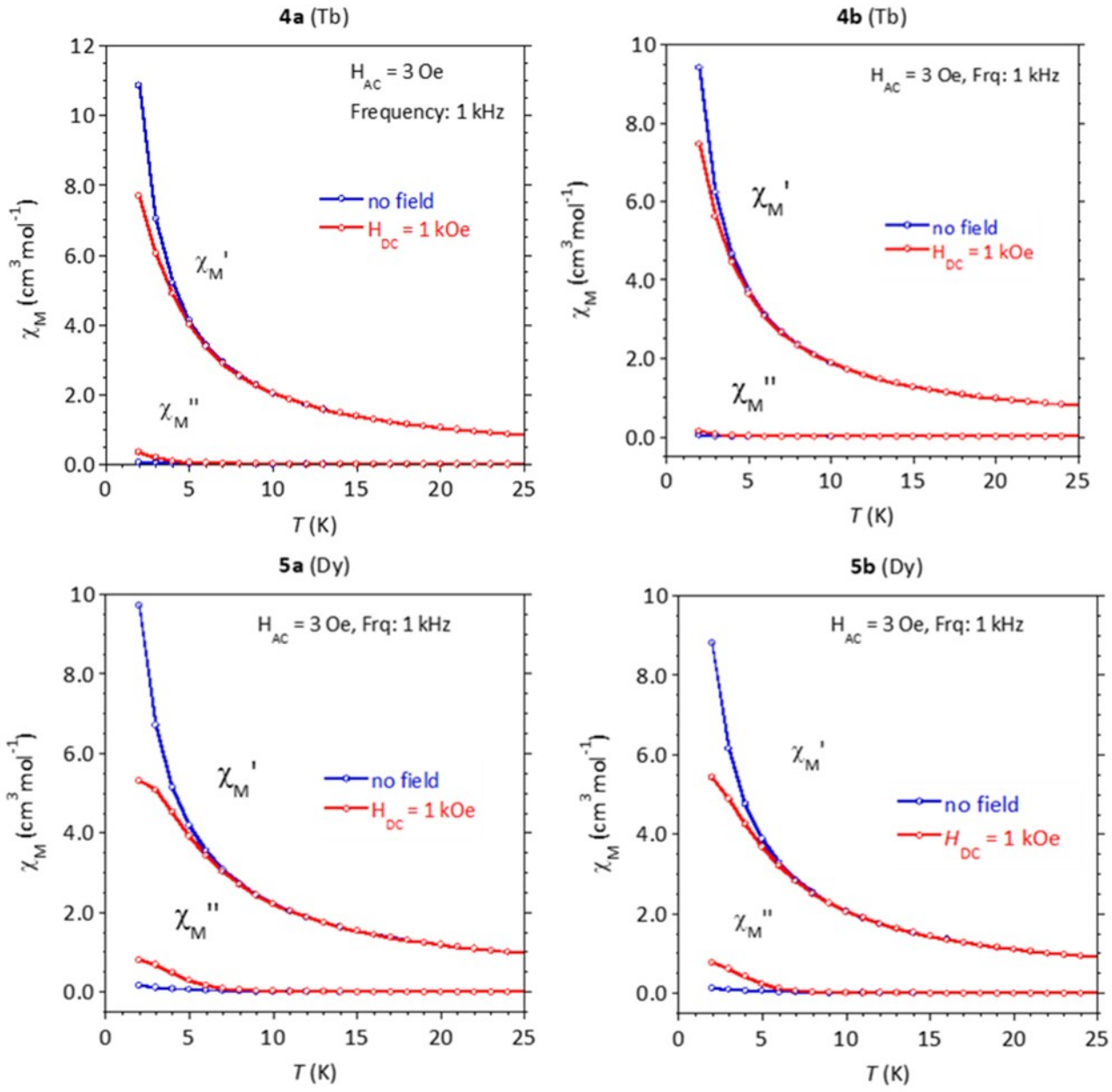

Figure S54. AC susceptibility behaviors for **4a, b** and **5a, b** in absence and with applied static magnetic field (H_{AC} = 3 Oe, ν = 1 kHz).

References:

1 K. Manna, B. Suresh Kumar, T. Maity and S. Natarajan, *ChemNanoMat*, 2022, **8**, e202200081.

2 T. P. Gerasimova and S. A. Katsyuba, *Dalt. Trans.*, 2013, **42**, 1787–1797.

3 A. Schweig and W. Thiel, *J. Electron Spectros. Relat. Phenomena*, 1974, **3**, 27–38.

4 M. M. Campos-Vallette, R. E. Clavijo, F. Mendizabal, W. Zamudio, R. Baraona and G. Diaz, *Vib. Spectrosc.*, 1996, **12**, 37–44.

5 P. G. Sammes and G. Yahioglu, *Chem. Soc. Rev.*, 1994, **23**, 327–334.

6 M. S. Henry and M. Z. Hoffman, *J. Phys. Chem.*, 1979, **83**, 618–625.

7 G. Accorsi, A. Listorti, K. Yoosaf and N. Armaroli, *Chem. Soc. Rev.*, 2009, **38**, 1690–1700.

8 S. Záliš, C. Consani, A. El Nahhas, A. Cannizzo, M. Chergui, F. Hartl and A. Vlček, *Inorganica Chim. Acta*, 2011, **374**, 578–585.

9 N. Sabbatini, M. Guardigli, I. Manet, F. Bolletta and R. Ziessel, *Inorg. Chem.*, 1994, **33**, 955–959.

10 Q.-Y. Yang, K. Wu, J.-J. Jiang, C.-W. Hsu, M. Pan, J.-M. Lehn and C.-Y. Su, *Chem. Commun.*, 2014, **50**, 7702–7704.

11 H. He, F. Sun, T. Borjigin, N. Zhao and G. Zhu, *Dalt. Trans.*, 2014, **43**, 3716–3721.

12 J.-C. Yin, Z. Chang, N. Li, J. He, Z.-X. Fu and X.-H. Bu, *ACS Appl. Mater. Interfaces*, 2020, **12**, 51589–51597.

13 L. Xu, Y. Xu, X. Li, Z. Wang, T. Sun and X. Zhang, *Dalt. Trans.*, 2018, **47**, 16696–16703.

14 R. Peña-Rodríguez, J. A. Molina-González, H. Desirena-Enrriquez, E. Armenta-Jaime, J. M. Rivera and S. E. Castillo-Blum, *J. Mater. Chem. C*, 2021, **9**, 15891–15899.

15 C. Y. Sun, X. L. Wang, X. Zhang, C. Qin, P. Li, Z. M. Su, D. X. Zhu, G. G. Shan, K. Z. Shao, H. Wu and J. Li, *Nat. Commun.*, 2013, **4**, 1–8.

16 L. L. da Luz, B. F. Lucena Viana, G. C. O. da Silva, C. C. Gatto, A. M. Fontes, M. Malta, I. T. Weber, M. O. Rodrigues and S. A. Júnior, *CrystEngComm*, 2014, **16**, 6914–6918.

17 D.-H. Chen, A. E. Sedykh, G. E. Gomez, B. L. Neumeier, J. C. C. Santos, V. Gvilava, R. Maile, C. Feldmann, C. WÖll, C. Janiak, K. Müller-Buschbaum and E. Redel, *Adv. Mater. Interfaces*, 2020, **7**, 2000929.

18 M.-L. Ma, C. Ji and S.-Q. Zang, *Dalt. Trans.*, 2013, **42**, 10579–10586.

19 Y. Wei, R. Sa and K. Wu, *Dalt. Trans.*, 2016, **45**, 18661–18667.

20 K. Manna, J.-P. Sutter and S. Natarajan, *Inorg. Chem.*, , DOI:10.1021/acs.inorgchem.2c02611.

21 M. L. Kahn, J.-P. Sutter, S. Golhen, P. Guionneau, L. Ouahab, O. Kahn and D. Chasseau, *J. Am. Chem. Soc.*, 2000, **122**, 3413–3421.

22 J. Sutter, M. L. Kahn and O. Kahn, *Adv. Mater.*, 1999, **11**, 863–865.

23 J. Sutter and M. L. Kahn, *Magn. Mol. to Mater. 5 Vol. Set*, 2004, 161–187.